NAVAL POSTGRADUATE SCHOOL

MONTEREY, CALIFORNIA

THESIS

PERFORMANCE ANALYSIS OF THE LINK-16/JTIDS WAVEFORM WITH CONCATENATED CODING

by

Ioannis Koromilas

September 2009

Thesis Advisor: Ralph C. Robertson
Second Reader: Terry Smith

REPORT DOCUMENTATION PAGE		*Form Approved OMB No. 0704-0188*

1. AGENCY USE ONLY *(Leave blank)*	**2. REPORT DATE** September 2009	**3. REPORT TYPE AND DATES COVERED** Master's Thesis	
4. TITLE AND SUBTITLE: Performance Analysis of the Link-16/JTIDS Waveform with Concatenated Coding		**5. FUNDING NUMBERS**	
6. AUTHOR Ioannis Koromilas			
7. PERFORMING ORGANIZATION NAME(S) AND ADDRESS(ES) Naval Postgraduate School Monterey, CA 93943-5000		**8.PERFORMING ORGANIZATION REPORT NUMBER**	
9. SPONSORING /MONITORING AGENCY NAME(S) AND ADDRESS(ES) N/A		**10. SPONSORING/MONITORING AGENCY REPORT NUMBER**	

12a. DISTRIBUTION / AVAILABILITY STATEMENT Approved for public release; distribution is unlimited	**12b. DISTRIBUTION CODE**

13. ABSTRACT (maximum 200 words)

Link-16 is the designation of a tactical data link that is being introduced into operations of the United States Navy, the Joint Services, and forces of the North Atlantic Treaty Organization (NATO). Link-16 does not significantly change the basic concepts of tactical data link information exchange, but rather provides certain technical and operational improvements to existing tactical data link capabilities. The communication terminal of Link-16 is called the Joint Tactical Information Distribution System (JTIDS) and features Reed-Solomon (RS) coding, symbol interleaving, cyclic code-shift keying (CCSK) for *M-ary* symbol modulation, minimum-shift keying (MSK) for chip modulation and combined frequency-hopping (FH) and direct sequence spread spectrum (DSSS) for transmission security. In this thesis, we investigate the performance of a Link-16/JTIDS-type waveform in both additive white Gaussian noise (AWGN) and pulsed-noise interference (PNI) when an alternative error correction coding scheme for the physical layer waveform is employed. The performance obtained using the alternative error correction coding scheme is compared to that of the existing JTIDS waveform when the same assumptions have been made for both waveforms. Based on the analyses, we conclude that the proposed alternative Link-16/JTIDS communication scheme performs better than the existing Link-16/JTIDS waveform in both AWGN and PNI for both coherent and noncoherent demodulation in terms of both required signal power and throughput.

14. SUBJECT TERMS Link-16/JTIDS, Reed-Solomon (RS) coding, Cyclic Code-Shift Keying (CCSK), Minimum-Shift Keying (MSK), convolutional codes, concatenated codes, perfect side information (PSI), Pulsed-Noise Interference (PNI), Additive White Gaussian Noise (AWGN), coherent detection, noncoherent detection.	**15. NUMBER OF PAGES** 101
	16. PRICE CODE

17. SECURITY CLASSIFICATION OF REPORT Unclassified	**18. SECURITY CLASSIFICATION OF THIS PAGE** Unclassified	**19. SECURITY CLASSIFICATION OF ABSTRACT** Unclassified	**20. LIMITATION OF ABSTRACT** UU

NSN 7540-01-280-5500

Standard Form 298 (Rev. 2-89)
Prescribed by ANSI Std. 239-18

THIS PAGE INTENTIONALLY LEFT BLANK

PERFORMANCE ANALYSIS OF THE LINK-16/JTIDS WAVEFORM WITH CONCATENATED CODING

Ioannis Koromilas
Lieutenant Junior Grade, Hellenic Navy
Bachelor of Naval Science, Hellenic Naval Academy, 2001

Submitted in partial fulfillment of the requirements
for the degree of

**MASTER OF SCIENCE IN ELECTRONIC WARFARE SYSTEMS
ENGINEERING**

from the

**NAVAL POSTGRADUATE SCHOOL
September 2009**

Author: Ioannis Koromilas

Approved by: Ralph C. Robertson
                Thesis Advisor

                Terry Smith
                Second Reader

                Dan C. Boger
                Chairman, Department of Information Sciences

iii

THIS PAGE INTENTIONALLY LEFT BLANK

ABSTRACT

Link-16 is the designation of a tactical data link that is being introduced into operations of the United States Navy, the Joint Services, and forces of the North Atlantic Treaty Organization (NATO). Link-16 does not significantly change the basic concepts of tactical data link information exchange, but rather provides certain technical and operational improvements to existing tactical data link capabilities. The communication terminal of Link-16 is called the Joint Tactical Information Distribution System (JTIDS) and features Reed-Solomon (RS) coding, symbol interleaving, cyclic code-shift keying (CCSK) for *M-ary* symbol modulation, minimum-shift keying (MSK) for chip modulation and combined frequency-hopping (FH), and direct sequence spread spectrum (DSSS) for transmission security. In this thesis, we investigate the performance of a Link-16/JTIDS-type waveform in both additive white Gaussian noise (AWGN), and pulsed-noise interference (PNI), when an alternative error correction coding scheme for the physical layer waveform is employed. The performance obtained using the alternative error correction coding scheme, is compared to that of the existing JTIDS waveform, when the same assumptions have been made for both waveforms.

Based on the analyses, we conclude that the proposed alternative Link-16/JTIDS communication scheme performs better than the existing Link-16/JTIDS waveform in both AWGN and PNI, for both coherent and noncoherent demodulation, in terms of both required signal power and throughput.

THIS PAGE INTENTIONALLY LEFT BLANK

TABLE OF CONTENTS

LIST OF FIGURES

x

LIST OF TABLES

THIS PAGE INTENTIONALLY LEFT BLANK

EXECUTIVE SUMMARY

Tactical data information links (TADIL) have played, and continue to play, a vital role in almost every modern battlefield, because the speed and accuracy of exchanged tactical information is of utmost importance for the outcome of the operations. In order to achieve their specified goal, the TADIL must have the ability to efficiently gather, manage, and relay all the data relevant to the tactical picture in a timely and accurate manner.

Link-16/Joint Tactical Information Distribution System (JTIDS) is a TADIL that is used in the operations of the United States Navy, the Joint Services, and forces of the North Atlantic Treaty Organization (NATO). Link-16 does not significantly change the basic concepts of tactical data link information exchange, but rather provides certain technical and operational improvements to previous tactical data link capabilities.

Link-16/JTIDS is a hybrid frequency-hopped (FH), direct sequence spread spectrum (DSSS) system, that utilizes a (31, 15) Reed-Solomon (RS) code and cyclic code-shift keying (CCSK) modulation for the data packets, where each encoded symbol consists of five bits. In this thesis, an alternative error correction coding scheme for the physical layer waveform of the JTIDS, that is consistent with the existing JTIDS error control coding scheme, was scrutinized. The system considered uses a concatenated code consisting of a rate $r = 4/5$ convolutional code as an outer code, and a $(31, k)$ RS code as an inner code. The coded symbols are transmitted on the in-phase (I) and quadrature (Q) components of the carrier using 32-*ary* CCSK. The performance obtained with the alternative error control coding scheme was compared with that obtained with the existing JTIDS waveform for the case where additive white Gaussian noise (AWGN) is the only noise present as well as when pulsed-noise interference (PNI) is present.

Based on the analyses and results of this thesis, we conclude that the proposed alternative Link-16/JTIDS compatible waveform yields the best performance when a (31, 23) RS code is used as an outer code, which results in a nearly 23% improvement in throughput as compared to the existing JTIDS waveform. We also observe that this

alternative encoding scheme requires less power than the existing Link-16/ JTIDS waveform for the same level of performance in both AWGN and PNI for coherent and noncoherent demodulation.

ACKNOWLEDGMENTS

I dedicate this work to my parents, Christo and Sofia, for their continuous love and support.

Also, I would like to thank Professor Clark Robertson for his guidance and patience during the work in performing this investigation.

THIS PAGE INTENTIONALLY LEFT BLANK

I. INTRODUCTION

A. OVERVIEW

Tactical data information links (TADIL) have played, and continue to play, a vital role in almost every modern battlefield because the speed and accuracy of exchanged tactical information is of utmost importance for the outcome of the operations. In order to achieve their specified goal, the TADIL must have the ability to efficiently gather, manage and relay all the relevant information of the tactical picture in a timely and accurate manner.

Link-16/Joint Tactical Information Distribution System (JTIDS) operates in the L-band and is a system developed to withstand hostile jamming. It uses a combination of time-division multiple access (TDMA), frequency-hopping (FH), direct sequence spread spectrum (DSSS), Reed-Solomon (RS) encoding, and cyclic code-shift keying (CCSK) modulation. Link-16/JTIDS produces a 32-chip sequence with CCSK modulation to represent each 5-bit symbol, and the individual chips are transmitted using minimum-shift keying (MSK) modulation.

A primary drawback to JTIDS is the limited data throughput, which reduces its effectiveness for the transmission of bulk data such as Intelligence, Surveillance and Reconnaissance (ISR) imagery or live video feeds. This constrains its usage to situational awareness functions, command and control, low data rate ISR functions, and derivative functions such as weapons guidance [1].

B. THESIS OBJECTIVE

Previous research has investigated various ways to improve either the robustness or the throughput, or both, of the JTIDS waveform. Modification of the modulation was considered in [2], while modification of both the modulation and the RS block length were considered in [3]. In [2], the robustness of the link was improved, but the throughput was not. In [3], both robustness and throughput were improved, but the cost would be a significant modification of the JTIDS transceiver.

1

The target of our research is to investigate an alternative error correction coding scheme for the physical layer waveform of the JTIDS that is consistent with the existing JTIDS error control coding scheme. The system considered uses a concatenated code consisting of a rate $r = 4/5$ convolutional code as an outer code, and a $(31, k)$ RS code as an inner code. The effects of both additive white Gaussian noise (AWGN) and pulsed-noise interference (PNI) are investigated. The performance for both coherent and noncoherent detection is analyzed. Also, no diversity, consistent with the single-pulse structure, and a sequential diversity of two, consistent with the JTIDS double-pulse structure, are both considered.

C. THESIS OUTLINE

The structure of this thesis is organized into the introduction, background (Chapter II) and five additional chapters. Chapter III contains an analysis of the performance of coherent and noncoherent 32-*ary* CCSK with concatenated coding in an AWGN environment. In Chapter IV, the performance of coherent and noncoherent 32-*ary* CCSK with concatenated coding in an AWGN and pulsed-noise interference (PNI) environment with no diversity is analyzed. Chapter V contains the performance analysis of coherent 32-*ary* CCSK with concatenated coding in an AWGN and PNI environment with a diversity of two. In Chapter VI, the performance analysis of noncoherent 32-*ary* CCSK with concatenated coding in an AWGN and PNI environment with a diversity of two is conducted assuming perfect side information (PSI). Finally, in Chapter VII the conclusions based on the results obtained from the analysis in the previous chapters are presented.

II.   BACKGROUND

In this chapter, some of the background knowledge and concepts required for the subsequent analysis of the alternative error correction coding scheme for the physical layer waveform of the JTIDS, considered in this thesis, are introduced.

A.   ALTERNATIVE LINK-16/JTIDS TYPE SYSTEM

The proposed Link-16/JTIDS features concatenated coding, bit-to-symbol and symbol-to-bit conversion, symbol interleaving, CCSK for *M-ary* baseband symbol modulation, MSK chip modulation for transmission and combined FH/DS spread spectrum for transmission security. The concatenated code consists of a rate $r = 4/5$, 2^8-state, convolutional code, and a (31, k) RS code. Based on [4], the physical layer (or transceiver) of the JTIDS-type system considered in this thesis is illustrated in Figure 1.
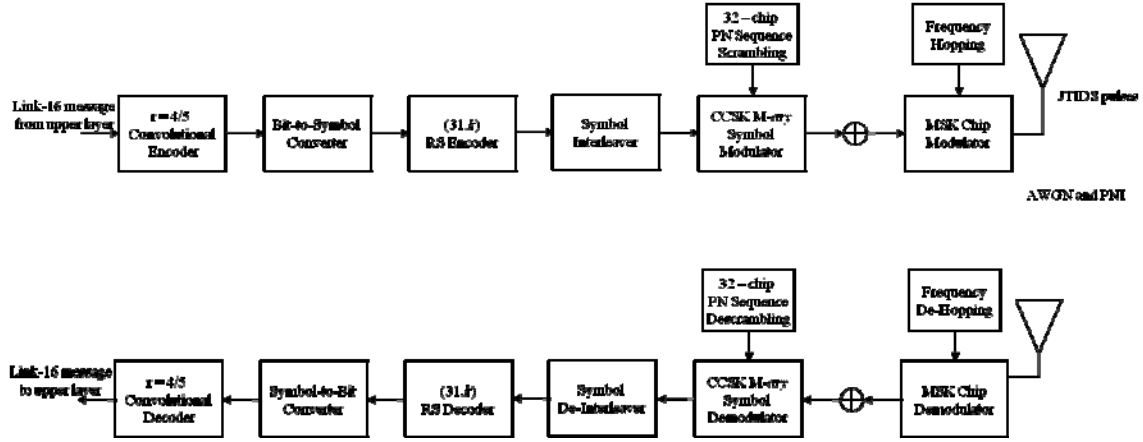
Figure 1.   A Link-16/JTIDS-type system model using the alternative error control coding scheme [After 4]

As seen in Figure 1, the top branch is the model of a Link-16/JTIDS-type transmitter using the alternative error control coding scheme, while the bottom branch is the model of the corresponding receiver. In addition to AWGN, pulsed-noise interference (PNI) is considered. Each functional block of Figure 1 is introduced block by block in this section.

1. Concatenated Codes

In a concatenated code, two codes, typically one binary and one nonbinary, are operated serially such that the codewords of the one code are treated as the input to the other code. Typically, a binary code is connected to the binary channel and called the inner code, and the nonbinary code, that operates on the combination of binary encoder/ binary channel/ binary decoder, is called the outer code. Because the JTIDS waveform is transmitted over a nonbinary channel, in this thesis, we reverse the normal order of binary and nonbinary codes.

To be more specific, let us consider the concatenated coding scheme shown in Figure 2. The binary (n,k) code forms the outer code, and the nonbinary code forms the inner code. The outer encoder takes k bits and generates an n-bit symbol. The inner, nonbinary code takes K n-bit symbols and generates N K-bit symbols. The result is an equivalent block code having a block length of Nn bits and containing kK information bits. Hence, the rate of the concatenated code is Kk / Nn, which is equal to the product of the code rates of the inner and outer codes.
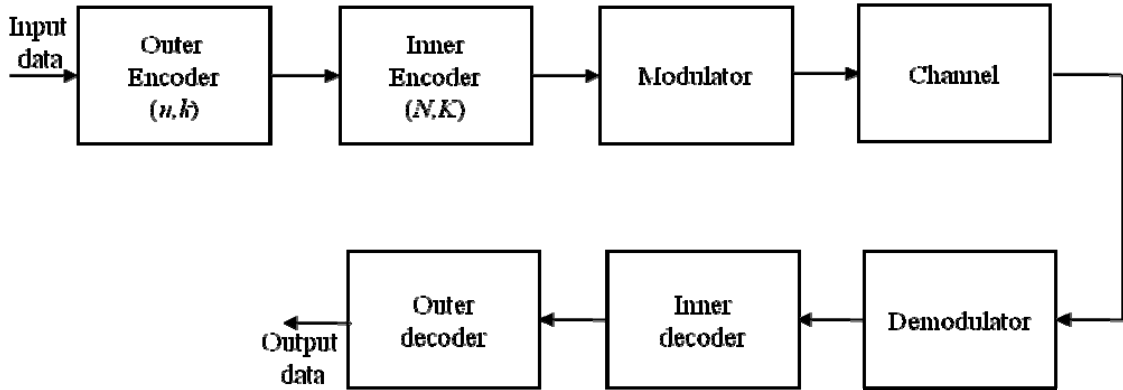
Figure 2.   A concatenated coding scheme [From [2]]

2. Convolutional Codes

Convolutional codes were first introduced by Elias [5] in 1955 as an alternative to block codes. Convolutional codes differ from block codes in that the encoder contains memory, and the encoder outputs at any given time unit depend not only on the inputs at that time unit but also on some number of previous inputs. A convolutional code is

4

generated by passing the information sequence to be transmitted through a linear finite-state shift register. In general, the shift register consists of K (k-bit) stages and n linear algebraic function generators, as shown in Figure 3. The input data to the encoder, which is assumed to be binary, is shifted into and along the shift register k bits at a time. The number of output bits for each k-bit input sequence is n bits. Consequently, the code rate is defined as $r = k/n$, consistent with the definition of the code rate for a block code. Typically, n and k are small integers, $k < n$, the information sequence is divided into blocks of length k, and the codeword is divided into blocks of length n. For the special case when $k = 1$, the information sequence is not divided into blocks and is processed continuously. Unlike with block codes, large minimum distances and low error probabilities are achieved not by increasing k and n but by increasing the number of states.
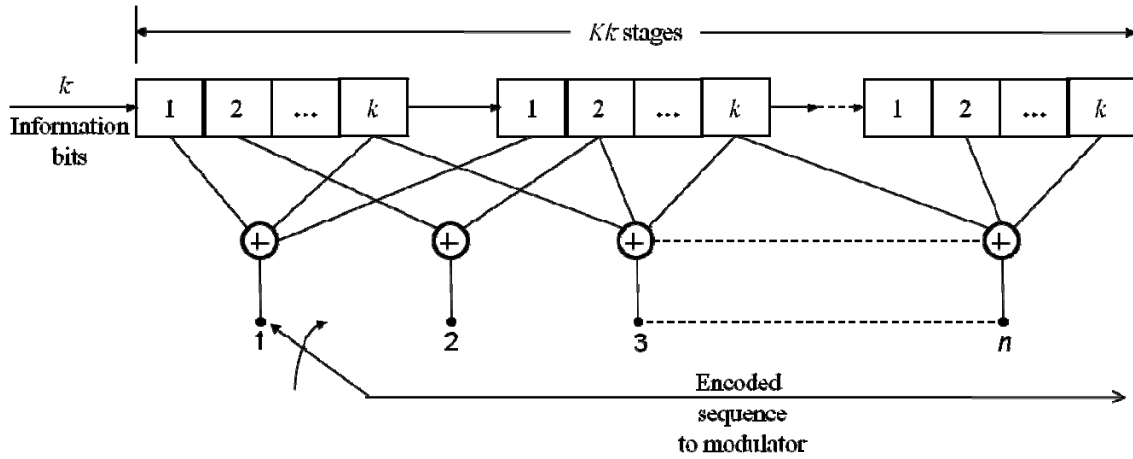
Figure 3.   Convolutional encoder [From 7]

In deriving the probability of bit error for convolutional codes, the linearity property for this class of codes is employed to simplify the derivation. That is, we assume that the all-zero sequence is transmitted, and we determine the probability of deciding in favor of another sequence. The pairwise error probability, when d is odd, is [7]

$$P_2(d) = \sum_{k=(d+1)/2}^{d} \binom{d}{k} p^k (1-p)^{n-k}, \qquad (2.1)$$

while, when d is even, the corresponding pairwise error probability $P_2(d)$ is [7]

5

$$P_2(d) = \frac{1}{2} \binom{d}{\frac{d}{2}} p^{d/2}(1-p)^{d/2} + \sum_{k=d/2+1}^{d} \binom{d}{k} p^k (1-p)^{n-k} \ . \tag{2.2}$$

where p is the channel probability of bit error and d is the Hamming distance between the selected code sequence and the correct code sequence.

Finally, the error probability is bounded by [7]

$$P_b \le \frac{1}{k} \sum_{d=d_{free}}^{\infty} \beta_d P_2(d), \tag{2.3}$$

where k is the number of the information bits of the convolutional code, d_{free} is the free distance of the convolutional code, and β_d represents the sum of all possible bit errors that can occur when the all-zero code sequence is transmitted.

3. Symbol-to-bit Conversion

The relationship between probability of bit error P_b and probability of symbol error P_E for an *M-ary* orthogonal signal set is [9]

$$\frac{P_b}{P_E} = \frac{2^{k-1}}{2^k - 1} = \frac{M/2}{M-1} . \tag{2.4}$$

4. Reed-Solomon (RS) Codes

RS codes are nonbinary Bose-Chaudhuri-Hocquenghem (BCH) codes, the most commonly used block codes for random error correction. For nonbinary codes, m bits at a time are combined to form a symbol, and $M = 2^m$ symbols are required to represent all possible combinations of m bits. An (n,k) RS encoder takes k information symbols and generates n coded symbols. RS codes have the largest possible minimum distance for each combination of n and k. A t-error correcting RS code with symbols from the Galois field of 2^m $(GF(2^m))$ is characterized by [7]

$$n = 2m - 1 \tag{2.5}$$
$$n - k = 2t \tag{2.6}$$
$$d_{min} = 2t + 1 \tag{2.7}$$

where t is the number of symbol errors that can be corrected and d_{min} is the minimum Hamming distance between any two code words. When AWGN is present, for orthogonal signaling, and hard decision decoding, the probability of symbol error for the RS codes is [10]

6

$$P_s \approx \frac{1}{n} \sum_{i=t+1}^{n} i \binom{n}{i} p_s^{\ i} (1-p_s)^{n-i}, \qquad (2.8)$$

where p_s is the probability of coded, or channel, symbol error, and t is the number of symbol errors guaranteed to be corrected in each block of n symbols.

5. Symbol Interleaver

A symbol interleaver is a device that mixes up the symbols from several different codewords so that the symbols from a specific codeword are not transmitted sequentially. A symbol de-interleaver in the receiver reverses the process, putting the received symbols back into proper order before passing them on to the decoder. For JTIDS, the symbol interleaver is used to interleave both the header symbols and data symbols. Because the header specifies the type of data and identifies the source track number of the transmitting terminal, the communications link could be significantly degraded if the header symbols are jammed.

6. Cyclic Code-shift Keying (CCSK) Baseband Symbol Modulation

Cyclic code-shift keying (CCSK) is a modulation technique that utilizes a single *M*-chip baseband waveform to represent *M* symbols. The *M*-chip baseband waveform represents the all-zero symbol, whereas all remaining combinations of k bits are represented by *M*–1 cyclical shifts of the initial *M*-chip baseband waveform. In Link-16/JTIDS, CCSK provides *M-ary* baseband modulation and spreading since each 5-bit symbol is represented by a 32-chip sequence. As shown in Figure 4, the 32-chip CCSK sequences are derived by cyclically shifting a starting sequence S_0 one place to the left between one and 31 times to obtain a unique sequence for all possible combinations of five bits.

DIRECTION OF SHIFT

5-Bit Symbol	32-Chip Sequence (CCSK Code Word)
00000	S0 = 01111100111010010000101011101100
00001	S1 = 11111001110100100001010111011000
00010	S2 = 11110011101001000010101110110001
00011	S3 = 11100111010010000101011101100011
00100	S4 = 11001110100100001010111011000111
•	
•	
•	
11111	S31 = 00111110011101001000010101110110

Figure 4.   The 32-chip CCSK sequences chosen for JTIDS [From 11]

After the CCSK symbol-to-chips spreading, each 32-chip CCSK sequence is scrambled with a 32-chip pseudo-noise (PN) sequence. This process not only provides a uniform spreading of the baseband waveform but also provides a second layer transmission security. The resulting 32-chip sequence is called a 32-chip transmission symbol.

An upper bound for the probability of symbol error for CCSK, in accordance with [12], is

$$P_S < \sum_{j=0}^{32} \zeta_{UB_j} \binom{32}{j} P_C^{\ j} (1-P_C)^{32-j},$$

(2.9)

where P_C is the probability of chip error at the output of the MSK chip demodulator and ζ_{UB_j} are the conditional probabilities of symbol error for CCSK sequence and are described in detail in [12]. The overall conditional probabilities of symbol error for the CCSK sequence chosen for JTIDS are listed in Table 1.

Table 1.   Conditional probabilities of symbol error for the CCSK sequence chosen by
            JTIDS. (From [12]).

$N = j$	ζ_{UB_j}
0	0
1	0
⋮	⋮
5	0
6	0
7	0.0015
8	0.0207
9	0.1166
10	0.4187
11	1.0
12	1.0
13	1.0
14	1.0
15	1.0
⋮	⋮
32	1.0

7.   Minimum-shift Keying (MSK) Chip Modulation

After scrambling, each chip is modulated for transmission using MSK modulation
scheme. MSK can be viewed as either a special case of continuous phase frequency-shift
keying (CPFSK), or a special case of offset quadrature phase-shift keying (OQPSK) with
sinusoidal symbol weighting [8]. MSK has many attractive attributes such as constant
envelope, compact spectrum, the error rate performance of binary phase-shift keying
(BPSK), and simple synchronization circuits.

B.   CHAPTER SUMMARY

In this chapter, the alternative error correction coding scheme for the physical
layer of the Link-16/JTIDS type system was introduced, and the background and
important concepts necessary to examine its performance were addressed. In Chapter III,
the performance analysis of coherent and noncoherent 32-*ary* CCSK with concatenated
coding in an AWGN environment is investigated.

THIS PAGE INTENTIONALLY LEFT BLANK

III. PERFORMANCE ANALYSIS OF COHERENT AND NONCOHERENT 32-ARY CCSK WITH CONCATENATED CODING IN AN AWGN ENVIRONMENT

In this chapter, we examine the performance of coherent and noncoherent 32-*ary* CCSK with concatenated coding in an AWGN environment.

For Link-16/JTIDS, data demodulation consists of two parts: MSK chip demodulation and CCSK symbol demodulation. The receiver structure of a Link-16/JTIDS-type system, using the alternative error correction coding scheme, is shown in Figure 1 and is reproduced here (Figure 5) for convenience. Given the assumptions that frequency de-hopping is perfectly synchronized with the frequency hopped waveform and that the signal-to-noise ratio is high enough, the MSK chip demodulator recovers the original 32-chip transmitted symbol. Given that de-scrambling is perfectly synchronized, the CCSK symbol demodulator detects the original 5-bit coded symbol. As seen in Figure 5, in order to evaluate the probability of information bit error P_b at the output of the convolutional decoder for a Link-16/JTIDS-type waveform using the alternative error correction coding scheme, the probability of channel chip error p_c at the output of the MSK chip demodulator, the probability of channel symbol error p_s at the output of the CCSK symbol demodulator, the probability of symbol error P_s at the output of RS decoder, and the probability of bit error p_b at the output of the symbol-to-bit converter all need to be evaluated.
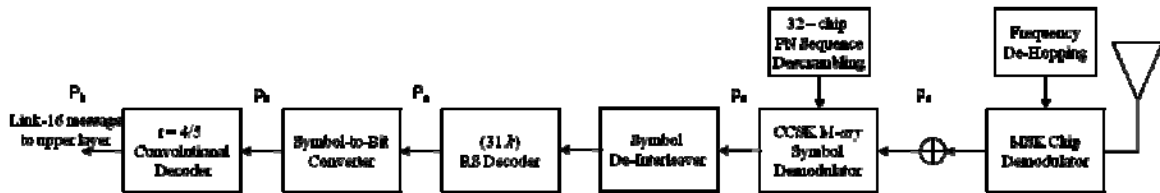
Figure 5.   Receiver structure of a Link-16/JTIDS-type system using the alternative error correction coding scheme [After 4]

11

We first examine the performance for coherent demodulation of the JTIDS waveform using the alternative error correction coding scheme in an AWGN environment, and subsequently, we analyze the performance for noncoherent demodulation of 32-*ary* CCSK using concatenated coding in an AWGN environment.

A. COHERENT DEMODULATION OF 32-ARY CCSK WAVEFORM IN AN AWGN ENVIRONMENT

1. Probability of Channel Chip Error

As mentioned in Chapter II, MSK can be considered as a special case of OQPSK with sinusoidal pulse shaping. When a coherent matched filter or correlator is used to recover the chips, MSK has the same performance as BPSK, QPSK and OQPSK [8]; that is,

$$P_c = Q\left(\sqrt{\frac{2E_c}{N_0}}\right), \tag{3.1}$$

where E_c is the average energy per chip, N_0 is the one-sided power spectral density (PSD) of the AWGN and $Q(x)$ is the Q-function, which is given by [8]

$$Q(x) = \frac{1}{2} erfc\left(\frac{x}{\sqrt{2}}\right), \tag{3.2}$$

and the complementary error function $erfc(x)$ is given by [8]

$$erfc(x) = \frac{2}{\sqrt{\pi}} \int_x^\infty \exp(-u^2) du. \tag{3.3}$$

Because each 5-bit symbol is converted into 32 chips,

$$E_s = 5E_b = 32E_c, \tag{3.4}$$

where E_s is the average energy per symbol and E_b is the average energy per bit. Therefore, equation (3.1) can be expressed as

$$P_c = Q\left(\sqrt{\frac{10E_b}{32N_0}}\right). \tag{3.5}$$

Note that Equation (3.5) is not the probability of channel chip error because forward error correction (FEC) coding has not been considered. Therefore, when FEC coding is applied, Equation (3.5) can be rewritten as

$$p_c = Q\left(\sqrt{\frac{10E_{b_c}}{32N_0}}\right) = Q\left(\sqrt{\frac{10rE_b}{32N_0}}\right). \tag{3.6}$$

where r is the rate of the concatenated code, E_{b_c} is the energy per coded bit and $E_{b_c} = rE_b$ [4].

2. Probability of Symbol Error

The probability of symbol error for the 32-*ary* CCSK used by JTIDS is given in equation (2.9) and is reproduced here for convenience

$$P_S = \sum_{j=0}^{32} \zeta_{UB_j} \binom{32}{j} P_C^{\,j}(1-P_C)^{32-j}. \tag{3.7}$$

Because the demodulation of CCSK symbol is independent of the FEC coding, the analytic expression for the probability of channel symbol error of a JTIDS/Link-16-type waveform can be obtained from Equation (3.7) by replacing P_S and P_C with p_s and p_c, respectively; that is,

$$p_s = \sum_{j=0}^{32} \zeta_{UB_j} \binom{32}{j} p_c^{\,j}(1-p_c)^{32-j}, \tag{3.8}$$

where ζ_{UB_j} are the conditional probabilities of channel symbol error given that j chip errors have occurred in the received, de-scrambled 32-chip sequence, and p_c is given by Equation (3.6).

3. Performance of Linear, Nonbinary Block Codes

As mentioned earlier, the alternative JTIDS will use a concatenated code for FEC coding, having a RS code as an inner code. A RS code is a linear, nonbinary block code. For a t-symbol error correcting, nonbinary block code, the probability of decoder, or block, error is upper bounded by [9]

$$P_E \le \sum_{i=t+1}^{n} \binom{n}{i} p_s^{\,i}(1-p_s)^{n-i}, \tag{3.9}$$

13

where the equality holds for a bounded distance decoder, and p_s is the probability of channel symbol error. Equation (3.9) can be used to obtain [9]

$$P_S \approx \frac{1}{n} \sum_{i=t+1}^{n} i \binom{n}{i} p_s^{\ i} (1 - p_s)^{n-i}. \tag{3.10}$$

Equation (3.10) can be used to evaluate the probability of symbol error of a JTIDS/Link-16-type waveform given the probability of channel symbol error p_s.

4.   Bit Error Probability versus Symbol Error Probability for Orthogonal Signals

As mentioned in Chapter II, the relationship between the probability of bit error and the probability of symbol error for an *M-ary* orthogonal signal set is [8]

$$\frac{P_b}{P_S} = \frac{2^{k-1}}{2^k - 1} = \frac{M/2}{M-1}, \tag{3.11}$$

which gives us the probability of bit error at the output of the symbol-to-bit converter.

5.   Performance of Convolutional Codes

In Chapter II, the probability of bit error for convolutional codes was evaluated and is reproduced here for convenience. The pairwise error probability when *d* is odd, is [7]

$$P_2(d) = \sum_{k=(d+1)/2}^{d} \binom{d}{k} P_b^{\ k} (1 - P_b)^{n-k}, \tag{3.12}$$

and the bit error probability is bounded by Equation (2.7), repeated here for convenience:

$$P_b \leq \frac{1}{k} \sum_{d=d_{free}}^{\infty} \beta_d P_2(d). \tag{3.13}$$

14

B. NONCOHERENT DEMODULATION OF 32-ARY CCSK WAVEFORM IN AN AWGN ENVIRONMENT

1. Probability of Channel Chip Error

MSK can also be noncoherently detected [8]. In that case the performance of MSK is identical to that of differential phase-shift keying (DPSK), which, when the optimum receiver is used, is [13]

$$P_C = \frac{1}{2} \exp\left(-E_C/N_0\right), \tag{3.14}$$

where E_C is the average energy per chip. Using Equation (3.4) in Equation (3.14), we get

$$P_C = \frac{1}{2} \exp(-10E_{b_c}/32N_0). \tag{3.15}$$

Note that Equation (3.15) is not the probability of channel chip error because FEC coding has not been considered. Therefore, when FEC coding is applied, Equation (3.15) must be rewritten as

$$P_C = \frac{1}{2} \exp\left(-10rE_b/32N_0\right), \tag{3.16}$$

where r is the code rate of the concatenated code.

C. PERFORMANCE ANALYSIS FOR COHERENT DEMODULATION OF 32-ARY CCSK WAVEFORM IN AN AWGN ENVIRONMENT

With Equations (3.6), (3.8), (3.10), (3.11), (3.12) and (3.13), we can investigate the probability of bit error of a Link-16/JTIDS-type waveform, using the alternative error control coding scheme and coherent demodulation. First, after using Equation (3.6) for different values of k, and therefore, different values of code rate r, for the concatenated code, in Equation (3.8), we obtain the probability of channel symbol error p_s. Afterwards, using Equation (3.8) in Equation (3.10), we obtain the probability of symbol error at the output of RS decoder. From Equation (3.11), we then obtain the probability of bit error at the input to the convolutional decoder. Finally, substituting Equation (3.11) in Equation (3.12) and Equation (3.12) into Equation (3.13), we obtain the probability of bit error at the receiver end. The results are shown in Figure 6. As can be seen, the best performance is achieved when RS (31, 23) is used, in which case in order to achieve bit

error probability $P_b = 10^{-5}$ the alternative waveform requires $E_b / N_0 = 5.9$ dB for coherent demodulation. Also we can see that the existing JTIDS at the same bit error probability of $P_b = 10^{-5}$ requires $E_b / N_0 = 7$ dB. In addition, there is an increase in system throughput on the order of 23%.
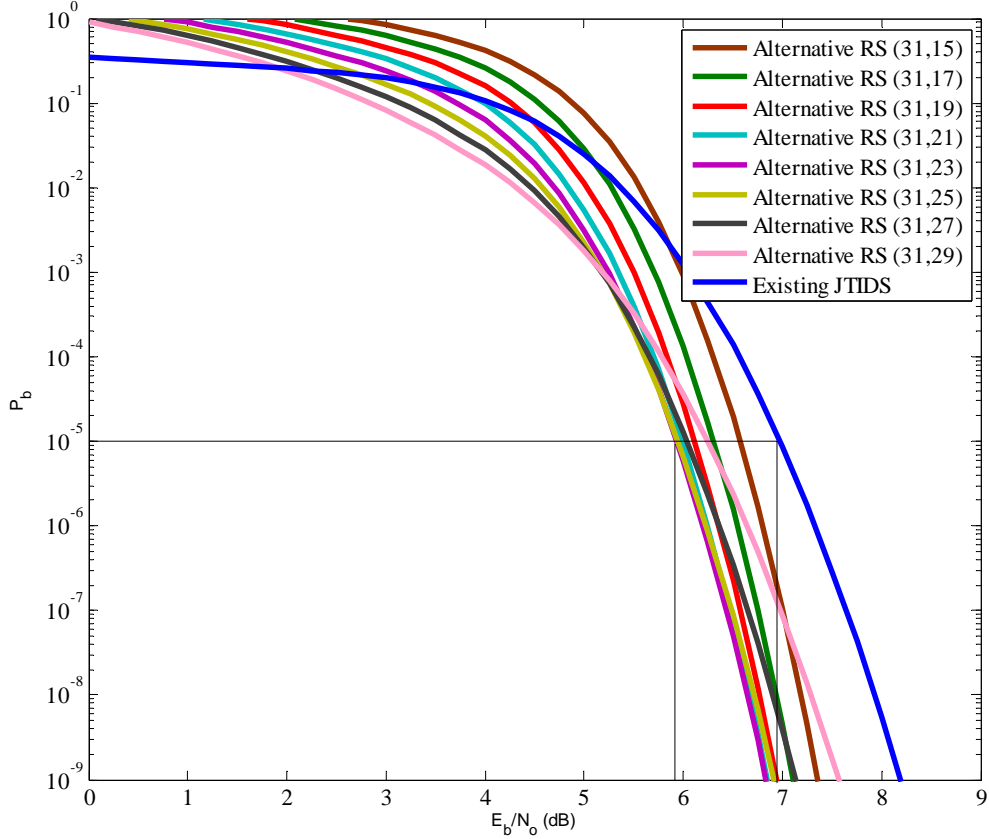
Figure 6.   Performance of 32-*ary* CCSK using the alternative error control coding scheme in AWGN for coherent demodulation and hard decision decoding.

D.   PERFORMANCE ANALYSIS FOR NONCOHERENT DEMODULATION OF 32-ARY CCSK WAVEFORM IN AN AWGN ENVIRONMENT

With Equations (3.8), (3.10), (3.11), (3.12), (3.13) and (3.16), we can similarly investigate the probability of bit error of a Link-16/JTIDS-type waveform using the alternative error control coding scheme with noncoherent detection. Repeating the procedure outlined in Section C but with Equation (3.16) instead of Equation (3.6), we

can obtain the information probability of bit error. The results are shown in Figure 7. As can be seen, the best performance is achieved when RS (31, 27) is used, in which case in order to achieve $P_b = 10^{-5}$ the alternative waveform requires $E_b / N_0 = 6.8$ dB for noncoherent demodulation. Also we can see that the actual JTIDS for $P_b = 10^{-5}$ requires $E_b / N_0 = 8$ dB. In this case, with noncoherent detection, there is a 31% increase in system throughput as opposed to a 23% increase with coherent detection.
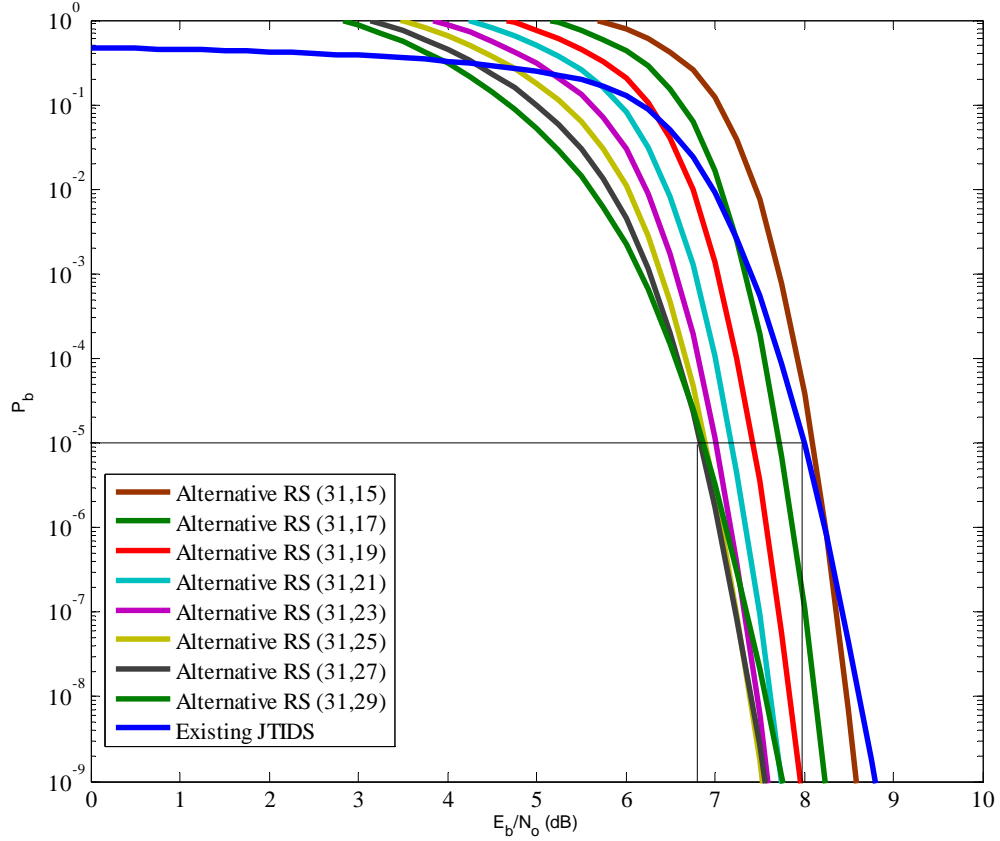
Figure 7.   Performance of 32-*ary* CCSK using the alternative error control coding scheme in AWGN for noncoherent demodulation and hard decision decoding.

E.   CHAPTER SUMMARY

In this chapter, the effects of AWGN on the performance for both coherent and noncoherent demodulation of the alternative error correction coding scheme, for the physical layer of JTIDS, were examined. In Chapter IV, the performance of JTIDS using the alternative error correction coding scheme for the physical layer for coherent and noncoherent demodulation in both AWGN and PNI are examined.

IV. PERFORMANCE ANALYSIS OF COHERENT AND NONCOHERENT 32-ARY CCSK WITH CONCATENATED CODING IN AN AWGN AND PNI ENVIRONMENT, WITH NO DIVERSITY

We now examine the performance of the receiver in the presence of pulsed-noise interference and AWGN. With PNI, we assume that the communications system is attacked by a noise-like signal that is turned on and off periodically. If ρ represents the fraction of time that the PNI is on, then $(1-\rho)$ represents the fraction of time that the PNI is turned off, where $0 < \rho \le 1$. In this kind of noisy environment, received symbols are affected by two different levels of noise power because some of the symbols are affected only by AWGN and the rest by both AWGN and PNI. If the one-sided power spectral density (PSD) of the AWGN is N_0 and the one-sided PSD of pulsed-noise interference is N_I when $\rho = 1$, then N_I/ρ is the PSD of the PNI because we assume that the average interference power is independent of ρ.

A. COHERENT DEMODULATION OF THE 32-ARY CCSK WAVEFORM IN AN AWGN AND PNI ENVIRONMENT, WITH NO DIVERSITY

When a Link-16/JTIDS-type waveform is subjected to both AWGN and PNI, Equation (3.13) can still be used to evaluate the probability of bit error because Equation (3.13) is independent of the types of noise and/or fading channels; however, the probability of channel symbol error p_s shown in Equation (3.8) must be modified using

$$p_s = \Pr\{\text{jammer off}\}\, p_s(\text{jammer off}) + \Pr\{\text{jammer on}\}\, p_s(\text{jammer on}) \quad (4.1)$$

because the probability of channel symbol error is determined at the symbol level instead of at the chip level and because a PNI environment is assumed. Equation (4.1) can be rewritten as

$$p_s = (1-\rho)p_{s_0} + \rho p_{s_1}, \quad (4.2)$$

where p_{s_0} is the probability of channel symbol error when the single-pulse is not jammed (PNI is off), and p_{s_1} is the probability of channel symbol error when the single-pulse is

jammed (PNI is on). Note that we assume that either all the chips of a symbol experience PNI or none of them do. The probability of channel symbol error when the single-pulse is not jammed is given by

$$p_{s_0} = \sum_{j=0}^{32} \zeta_{UBj} \binom{32}{j} p_{c_0}{}^j (1 - p_{c_0})^{32-j} \tag{4.3}$$

where ζ_{UBj} are the conditional probabilities of channel symbol error given that j chip errors have occurred in the received, de-scrambled 32-chip sequence. The probability of channel chip error when the single-pulse is not jammed, is given by

$$p_{c_0} = Q\left(\sqrt{\frac{10rE_b}{32N_0}} \right), \tag{4.4}$$

where r is the code rate. Similarly, the probability of channel symbol error when the single-pulse is jammed is given by

$$p_{s_1} = \sum_{j=0}^{32} \zeta_{UBj} \binom{32}{j} p_{c_1}{}^j (1 - p_{c_1})^{32-j}, \tag{4.5}$$

where p_{c_1} is the probability of channel chip error when the single-pulse is jammed, given by

$$p_{c_1} = Q\left(\sqrt{\frac{10rE_b}{32(N_0 + N_I/\rho)}} \right). \tag{4.6}$$

The effect of PNI is to increase the noise PSD by $1/\rho$ if a constant average interference power is assumed.

Now, using Equation (4.4) for different code rates r in Equation (4.3), we obtain the probability of channel symbol error when the single-pulse is not jammed p_{s_0}. Similarly, using Equation (4.6) for different code rates r and values of ρ in Equation (4.5), we obtain the probability of channel symbol error when the single-pulse is jammed p_{s_1}. Next, substituting p_{s_0} and p_{s_1} into Equation (4.2), we obtain the average probability of channel symbol error p_s. Substituting the average probability of channel symbol error p_s into Equation (3.10), we obtain the probability of symbol error at the output of the RS decoder. Now, using Equation (3.11) we obtain the probability of bit error at the output of

symbol-to-bit converter p_b. Finally, substituting the bit error probability p_b in Equation (3.12) and substituting Equation (3.12) into Equation (3.13), we obtain the probability of bit error P_b of a Link-16/JTIDS-type waveform using the alternative error correction coding scheme for the physical layer for the single-pulse structure in both AWGN and PNI.

The performance of the alternative waveform, as well as that of the existing Link-16/JTIDS, for different values of ρ and different code rates r of the concatenated code for coherent demodulation, are shown in Figures 8–15. From the plots, we see that PNI degrades the performance of the system relative to barrage-noise interference (BNI) $(\rho = 1)$. We also observe that the higher rate codes yield better performance for higher values of the ratio of bit energy-to-noise power spectral density (E_b / N_0), whereas smaller rate codes show better performance for small values of E_b / N_0.

From Table 2, we can see that PNI degrades the performance of the alternative system relative to BNI $(\rho = 1)$ when $P_b = 10^{-5}$ by 1.4 dB, whereas the actual JTIDS performance is degraded by 1.5 dB. We should note that in this table the alternative waveform that yields the best performance for each case under investigation has been used. For $\rho \leq 0.1$ and $E_b / N_0 = 10$ dB, the performance of the alternative waveform is not affected by PNI for $P_b \geq 10^{-5}$, while actual JTIDS performance is not affected by PNI for $P_b \geq 10^{-5}$ and $E_b / N_0 = 10$ dB when $\rho < 0.1$. Also we observe that in each case the performance of the alternative waveform is generally superior to that of the original JTIDS. Indeed that superiority becomes more evident for $\rho \leq 0.1$. The reader should also note that this improvement in required received signal power does not come at the expense of reduced throughput. Indeed, throughput is increased, particularly when $\rho = 1$ and $\rho = 0.5$.

Table 2.   Performance of 32-*ary* CCSK with the concatenated code for different values of ρ in both AWGN and PNI for coherent demodulation, hard decision decoding and $E_b / N_0 = 10$ dB.

P_b	ρ	**Waveform**	E_b / N_I **(dB)** **(Existing JTIDS)**	E_b / N_I **(dB)** **(Alternative Waveform)**
10^{-5}	1	Alternative RS(31,23)	10	8
10^{-5}	0.5	Alternative RS(31,21)	11.1	9.4
10^{-5}	0.1	Alternative RS(31,19)	11.5	0
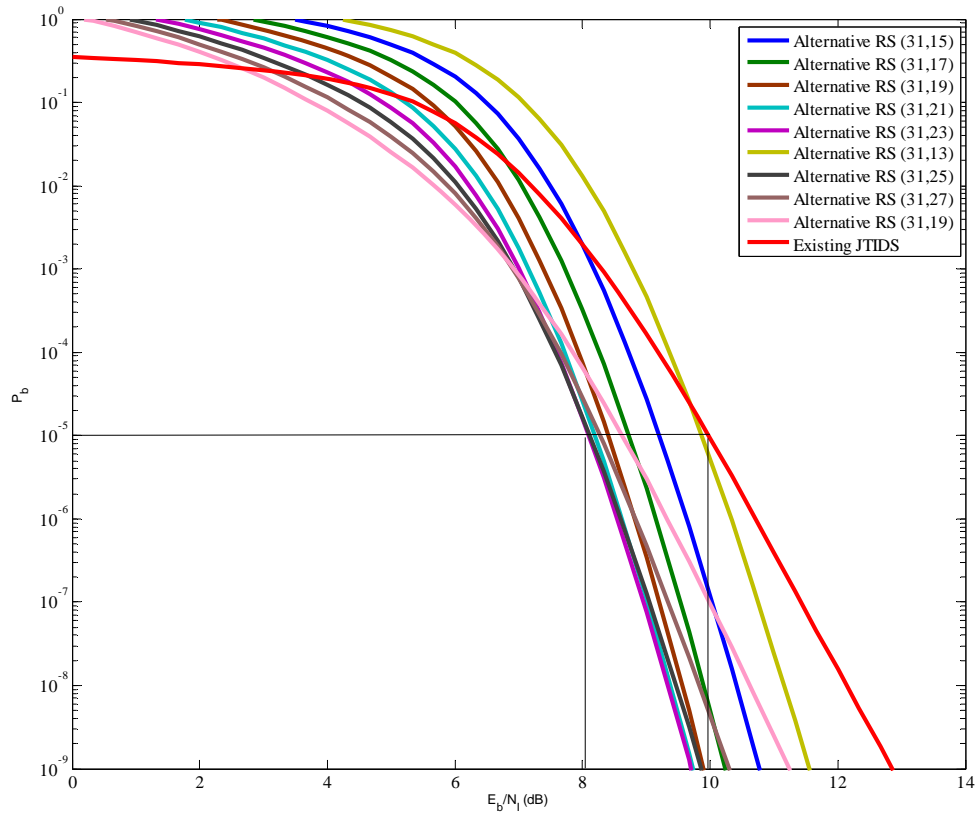
Figure 8.   Performance of 32-*ary* CCSK using concatenated coding in both AWGN and PNI for $\rho=1$, coherent demodulation, hard decision decoding and $E_b / N_0 = 10$ dB.
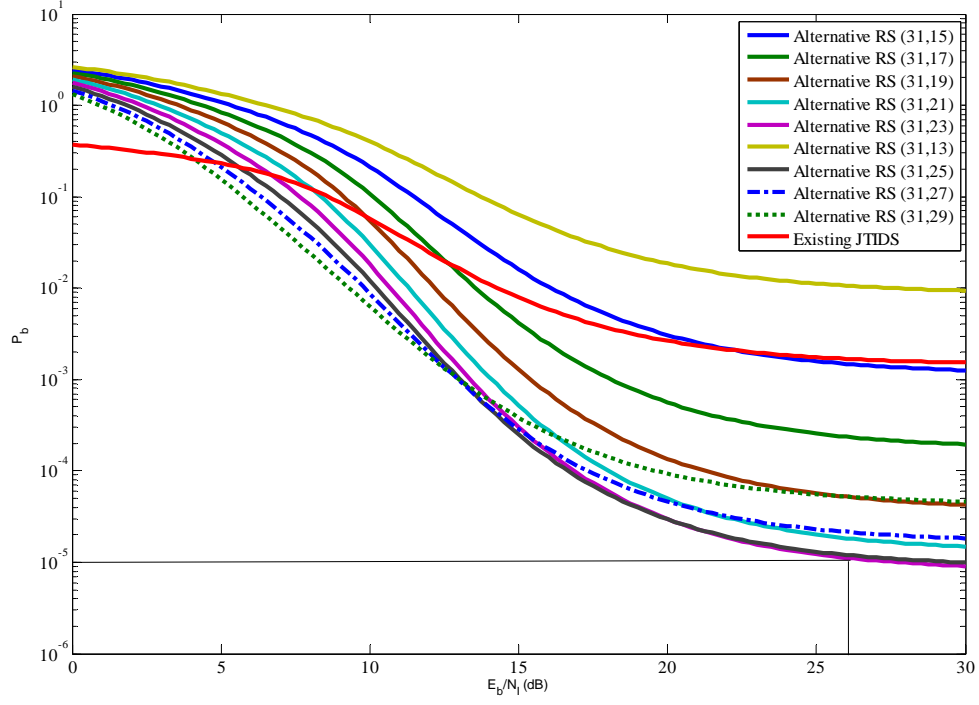
Figure 9. Performance of 32-*ary* CCSK using concatenated coding in both AWGN and PNI for ρ=1, coherent demodulation, hard decision decoding and $E_b / N_0 = 6$ dB.
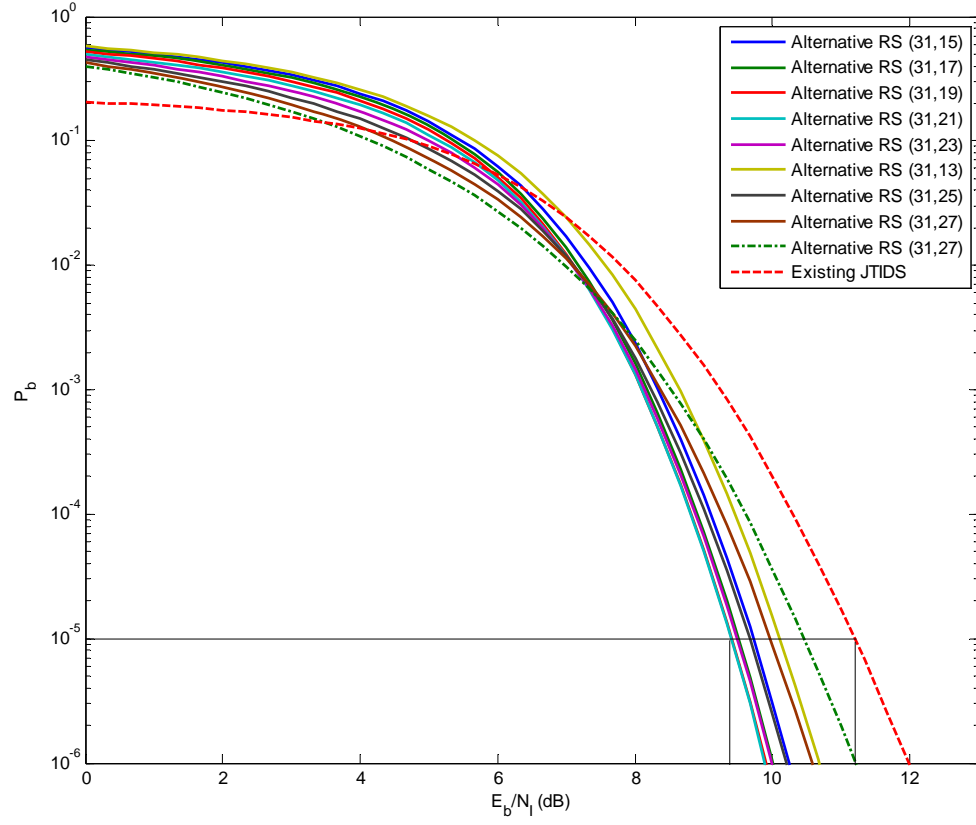
Figure 10. Performance of 32-*ary* CCSK using concatenated coding in both AWGN and PNI for ρ=0.5, coherent demodulation, hard decision decoding and $E_b / N_0 = 10$ dB.
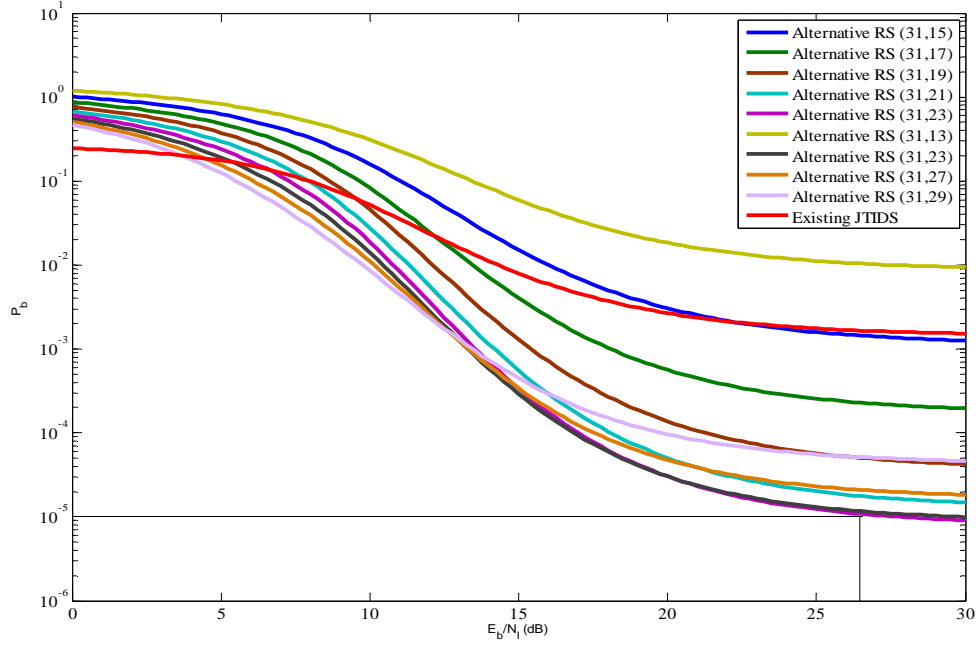
Figure 11.   Performance of 32-*ary* CCSK using concatenated coding in both AWGN and PNI for ρ=0.5, coherent demodulation, hard decision decoding and $E_b / N_0 = 6$ dB.
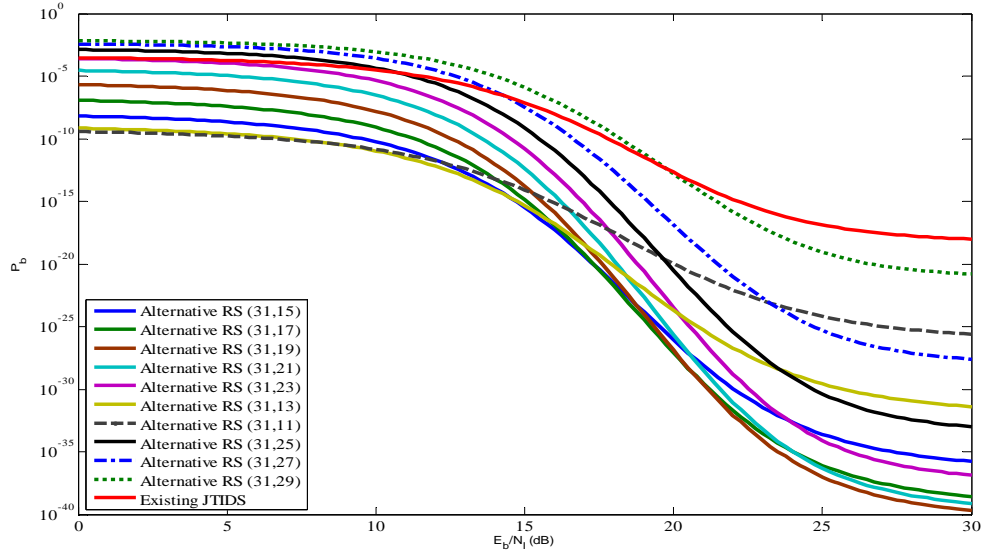
Figure 12.   Performance of 32-*ary* CCSK using concatenated coding in both AWGN and PNI for ρ=0.1, coherent demodulation, hard decision decoding and $E_b / N_0 = 10$ dB.

Figure 13.   Performance of 32-*ary* CCSK using concatenated coding in both AWGN and PNI for ρ=0.1, coherent demodulation, hard decision decoding and $E_b / N_0 = 6$ dB.

Figure 14.   Performance of 32-*ary* CCSK using concatenated coding in both AWGN and PNI for ρ=0.01, coherent demodulation, hard decision decoding and $E_b / N_0 = 10$ dB.

Figure 15.   Performance of 32-*ary* CCSK using concatenated coding in both AWGN and PNI for $\rho=0.01$, coherent demodulation, hard decision decoding and $E_b / N_0 = 6$ dB.

B.   NONCOHERENT DEMODULATION OF THE 32-ARY CCSK WAVEFORM IN AN AWGN AND PNI ENVIRONMENT, WITH NO DIVERSITY

Following the same approach as in the coherent case, we find the probability of channel symbol error p_s as given by Equation (4.2), which is reproduced here for convenience:

$$p_s = (1-\rho)p_{s_0} + \rho p_{s_1},\tag{4.7}$$

where p_{s_0} is the probability of channel symbol error when the single-pulse is not jammed (PNI is off), and p_{s_1} is the probability of channel symbol error when the single-pulse is jammed (PNI is on). The probability of channel symbol error when the single-pulse is not jammed is given by Equation (4.3), which is reproduced here for convenience:

$$p_{s_0} = \sum_{j=0}^{32} \zeta_{UBj} \binom{32}{j} p_{c_0}{}^j (1-p_{c_0})^{32-j},\tag{4.8}$$

27

where ζ_{UBj} are the conditional probabilities of channel symbol error given that j chip errors have occurred in the received, de-scrambled 32-chip sequence. The probability of channel chip error when the single-pulse is not jammed, given by Equation (3.14), is reproduced here for convenience:

$$p_{c_0} = \frac{1}{2}\exp\left(-10rE_b/32N_0\right),\tag{4.9}$$

where r is the rate of the concatenated code. Similarly, the probability of channel symbol error when the single-pulse is jammed is given by

$$p_{s_1} = \sum_{j=0}^{32} \zeta_{UBj}\binom{32}{j}p_{c_1}{}^{j}(1-p_{c_1})^{32-j},\tag{4.10}$$

where p_{c_1} is the probability of channel chip error when the single-pulse is jammed, given by

$$p_{c_1} = \frac{1}{2}\exp\left(\frac{-10rE_b}{32(N_0 + N_I/\rho)}\right).\tag{4.11}$$

Now, using Equation (4.9) for different code rates r in Equation (4.8), we obtain the probability of channel symbol error when the single-pulse is not jammed p_{s_0}. Similarly, using Equation (4.11) for different code rates r and values of ρ in Equation (4.10), we obtain the probability of channel symbol error when the single-pulse is jammed p_{s_1}. Next, substituting p_{s_0} and p_{s_1} into Equation (4.7), we obtain the average probability of channel symbol error p_s. Now substituting the average probability of channel symbol error p_s into Equation (3.10), we obtain the probability of symbol error at the output of the RS decoder. Using Equation (3.11), we obtain the probability of bit error at the output of symbol-to-bit converter p_b. Finally, substituting the bit error probability p_b into Equation (3.12) and substituting Equation (3.12) into Equation (3.13), we obtain the probability of bit error P_b of a Link-16/JTIDS-type system using the alternate error correction coding scheme for the physical layer for the single-pulse structure in both AWGN and PNI for noncoherent demodulation. The results are shown in Figures 16 through 23. From the plots, we see that PNI degrades the performance of

the system relative to BNI $(\rho = 1)$. We also observe that the higher rate codes yield better performance for higher values of E_b / N_0, whereas smaller rate codes show better performance for small values of E_b / N_0.

From Table 3 we can see that PNI degrades the performance of the alternative system relative to BNI $(\rho = 1)$ when $P_b = 10^{-5}$ by 2 dB, whereas the actual JTIDS performance is degraded by 1.5 dB. We should note that the table entries are the alternative waveforms that yield the best performance for each case under investigation. For $\rho \leq 0.1$ and $E_b / N_0 = 10$ dB, the performance of the alternative waveform is not affected for $P_b = 10,^{-5}$ just as in the case of coherent detection, while actual JTIDS performance is not affected for $P_b = 10^{-5}$ and $E_b / N_0 = 10$ dB when $\rho < 0.1$. Also we observe that in each case the performance of the alternative waveform is superior to that of the original JTIDS. Indeed that superiority becomes more evident for $\rho \leq 0.1$.

Table 3. Performance of 32-*ary* CCSK with the concatenated code for different values of ρ in both AWGN and PNI for noncoherent demodulation, hard decision decoding and $E_b / N_0 = 10$ dB.

| P_b	ρ	Waveform	E_b / N_I (dB) (Existing JTIDS)	E_b / N_I (dB) (Alternative Waveform)
10^{-5}	1	Alternative RS(31,27)	15.7	9.7
10^{-5}	0.5	Alternative RS(31,25)	16.6	11.7
10^{-5}	0.1	Alternative RS(31,15)	18	0
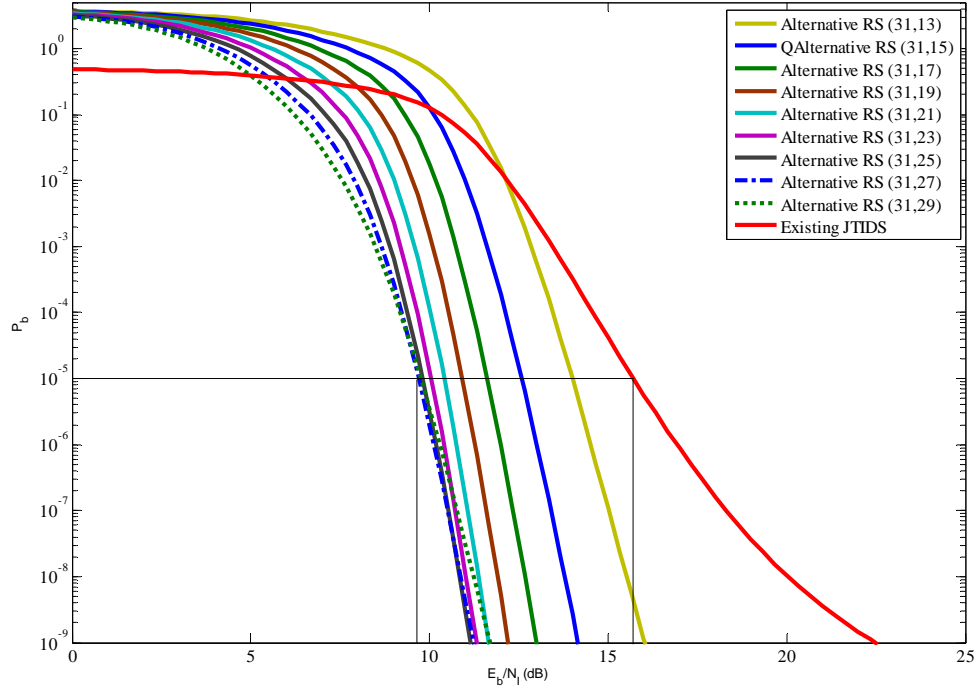
Figure 16.   Performance of 32-*ary* CCSK using concatenated coding in both AWGN and PNI for ρ=1, noncoherent demodulation, hard decision decoding and $E_b / N_0 = 10$ dB.
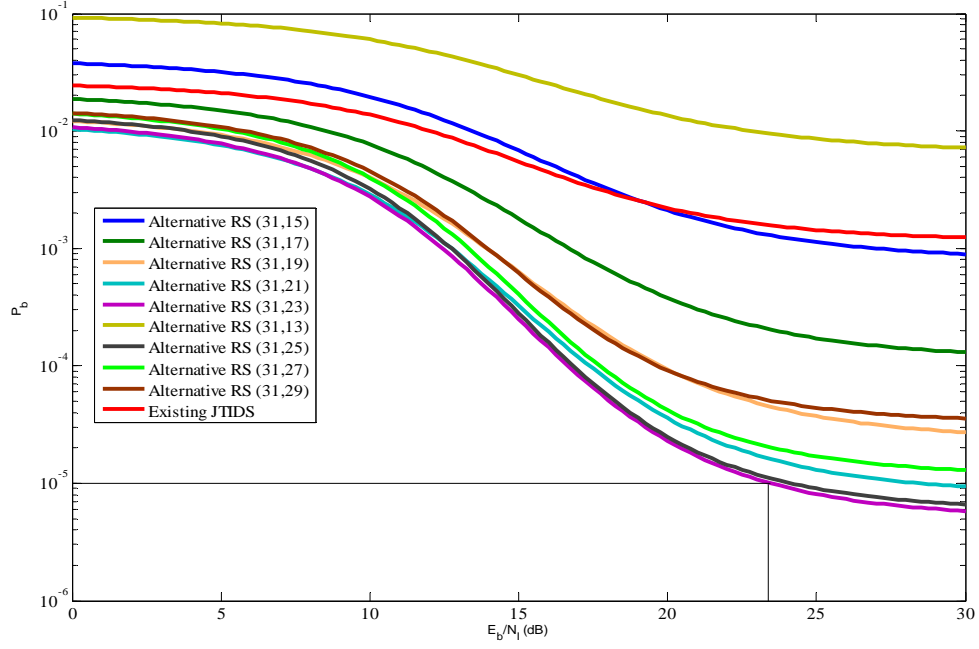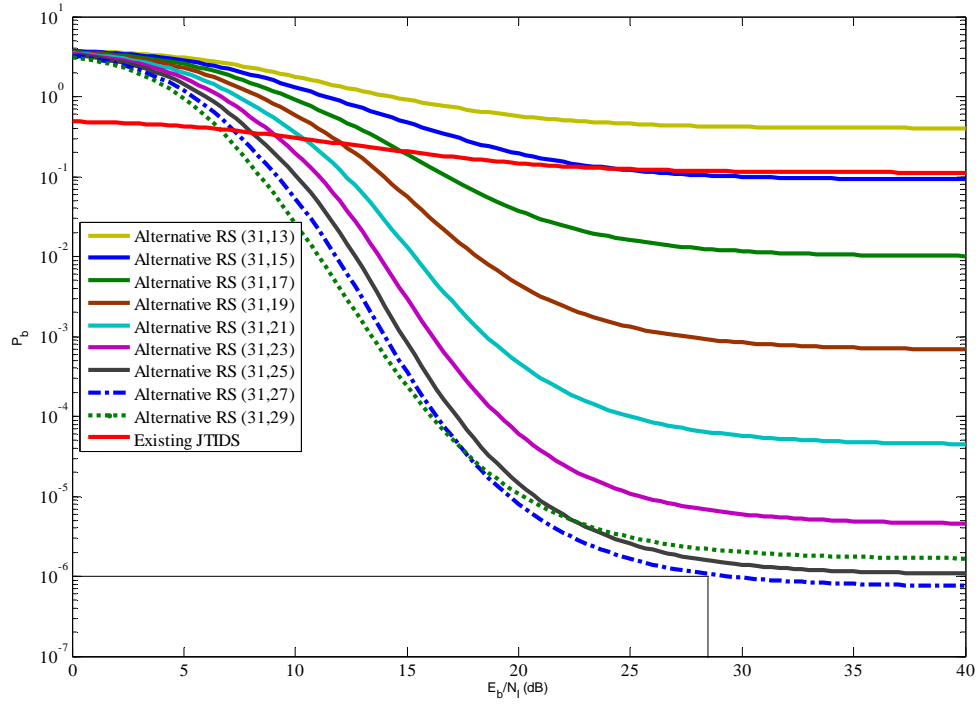
Figure 17.   Performance of 32-*ary* CCSK using concatenated coding in both
AWGN and PNI for ρ=1, noncoherent demodulation, hard decision
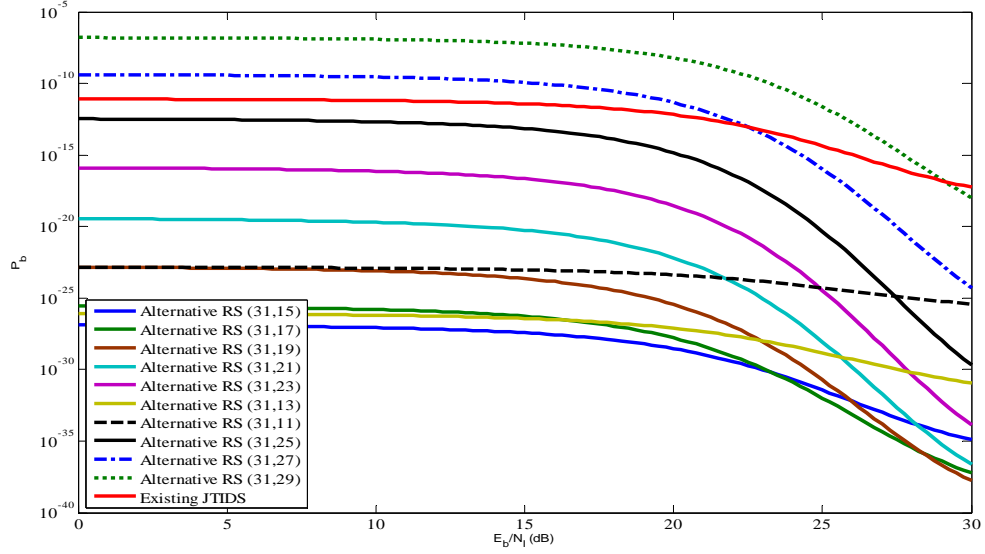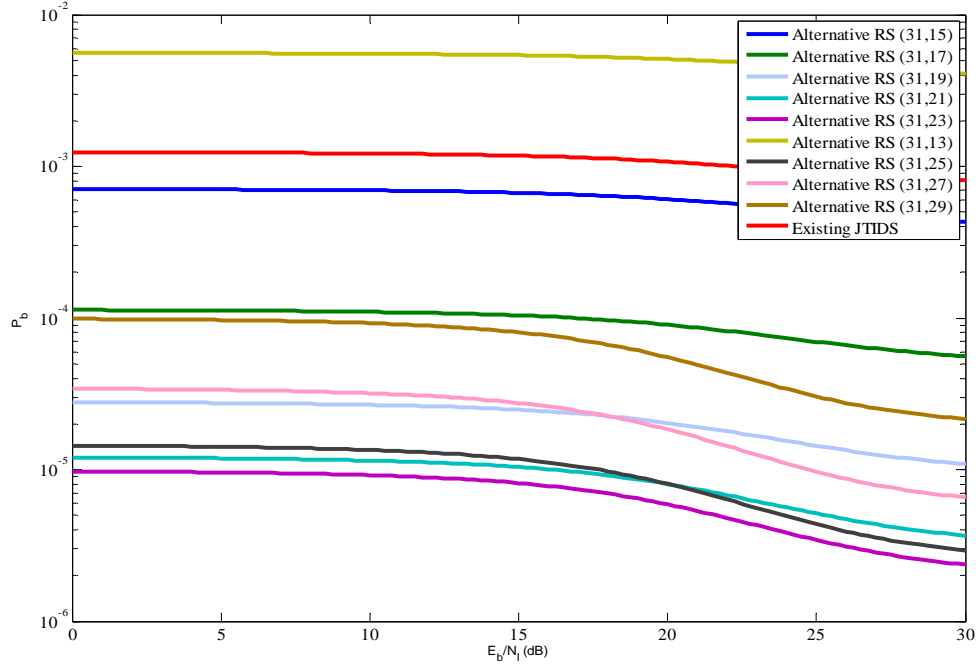decoding and $E_b / N_0 = 6.9$ dB.
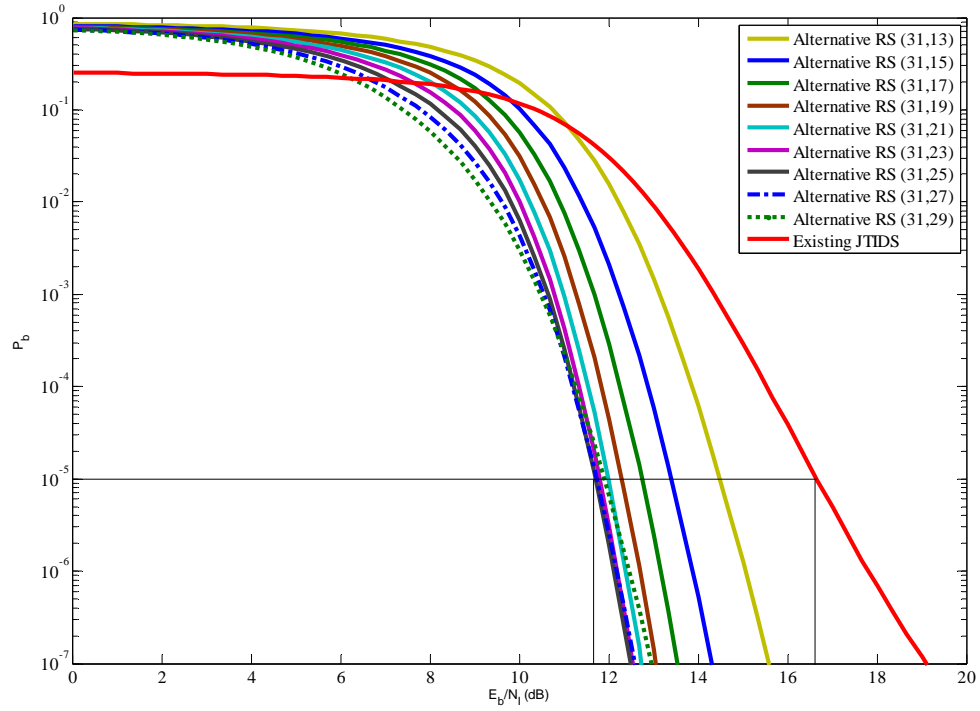
Figure 18. Performance of 32-*ary* CCSK using concatenated coding in both AWGN and PNI for ρ=0.5, noncoherent demodulation, hard decision decoding and $E_b / N_0 = 10$ dB.
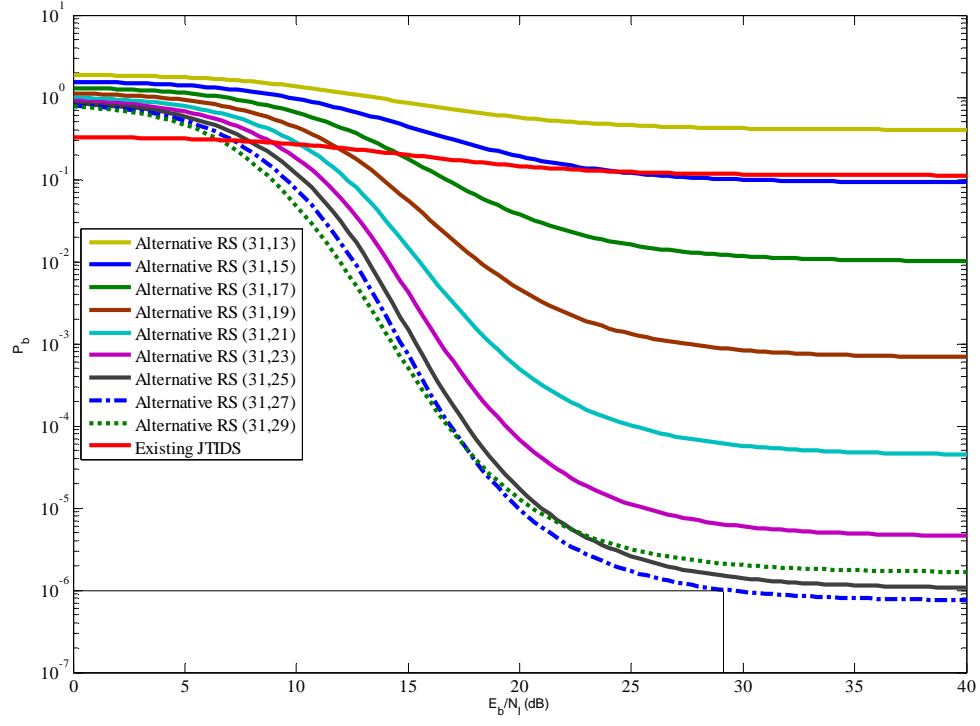
Figure 19.   Performance of 32-*ary* CCSK using concatenated coding in both
AWGN and PNI for ρ=0.5, noncoherent demodulation, hard decision
decoding and $E_b / N_0 = 7.1$ dB.
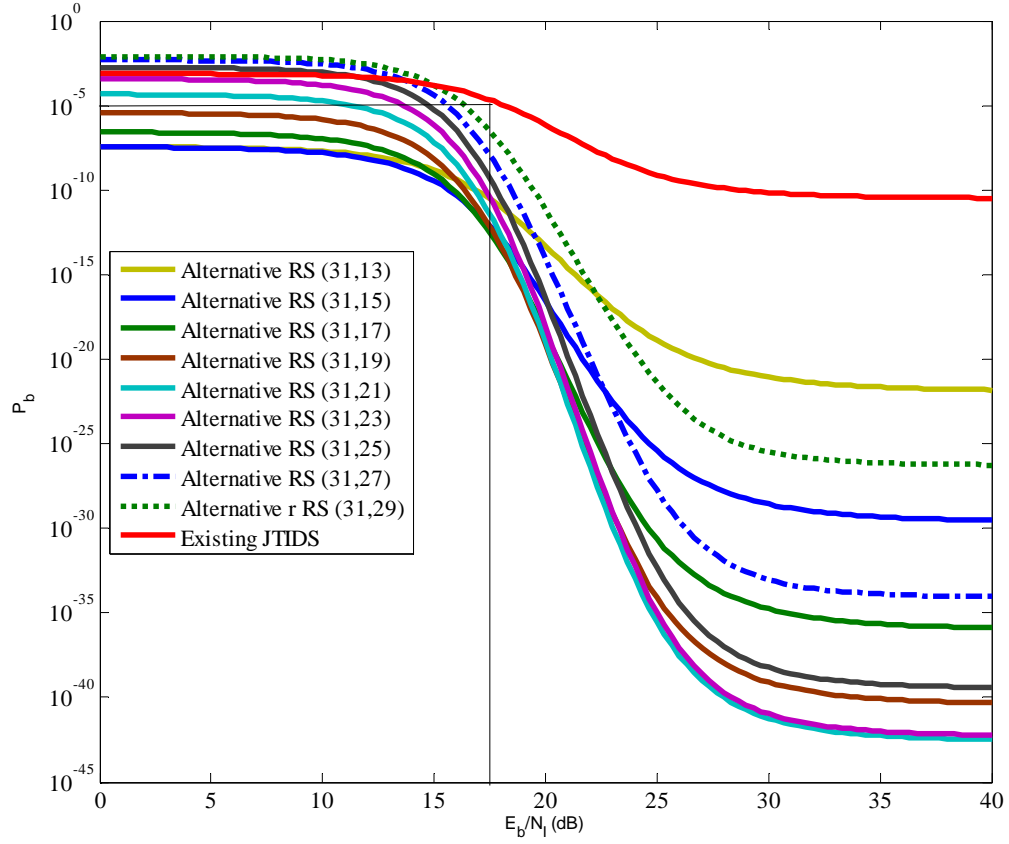
Figure 20.   Performance of 32-*ary* CCSK using concatenated coding in both
AWGN and PNI for ρ=0.1, noncoherent demodulation, hard decision
decoding and $E_b / N_0 = 10$ dB.
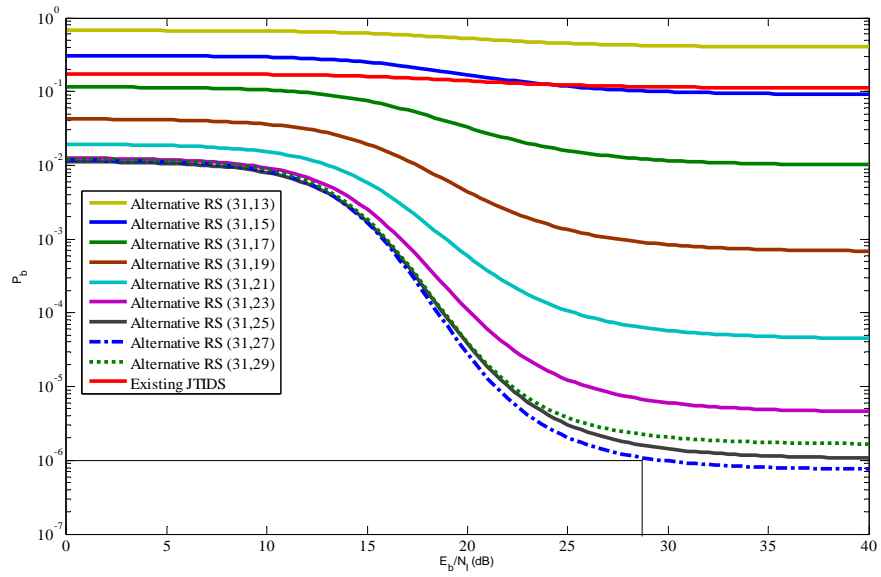
Figure 21.   Performance of 32-*ary* CCSK using concatenated coding in both AWGN and PNI for ρ=0.1, noncoherent demodulation, hard decision decoding and $E_b / N_0 = 7.1$ dB.
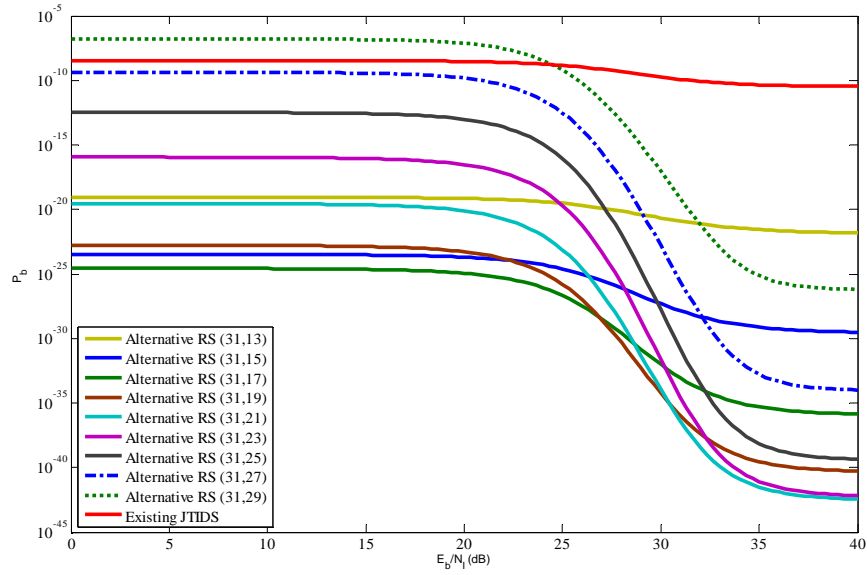
Figure 22.   Performance of 32-*ary* CCSK using concatenated coding in both AWGN and PNI for ρ=0.01, noncoherent demodulation, hard decision decoding and $E_b / N_0 = 10$ dB.
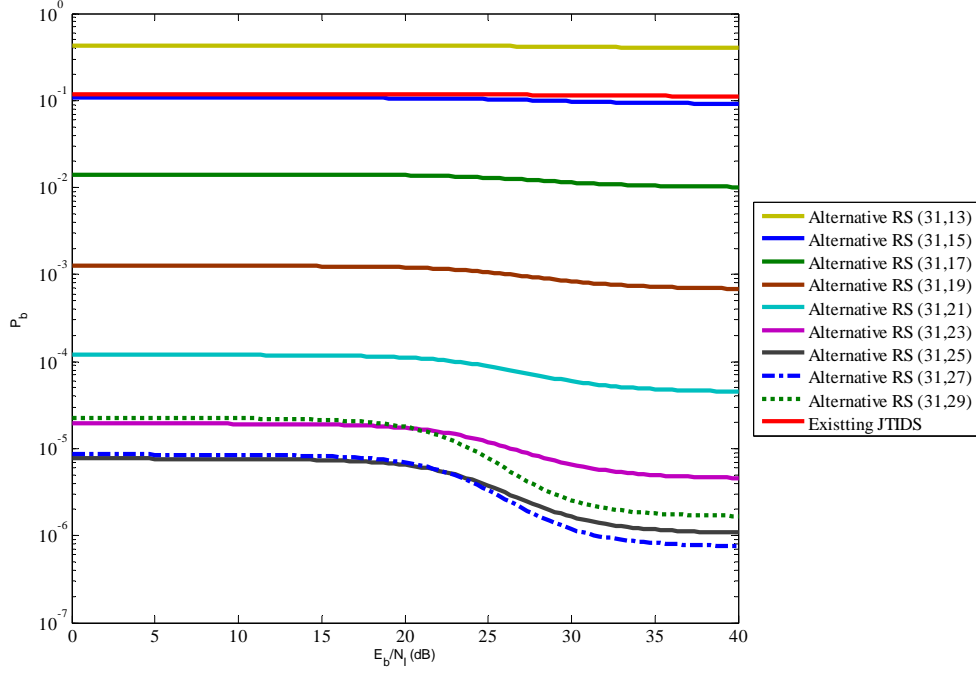
Figure 23. Performance of 32-*ary* CCSK using concatenated coding in both AWGN and PNI for ρ=0.01, noncoherent demodulation, hard decision decoding and $E_b / N_0 = 7.1$ dB.

C. COMPARISON BETWEEN COHERENT AND NONCOHERENT DEMODULATION

For purposes of comparison, the performance for both coherent and noncoherent demodulation of the alternative waveform for ρ=1, ρ=0.5 and ρ=0.1 are plotted in Figures 24, 25 and 26 respectively. In each figure, we use two values for E_b / N_0, namely 10 dB and 7.1 dB. The value of 7.1 dB was chosen because this results in $P_b = 10^{-6}$ for noncoherent demodulation when $E_b / N_I \gg 1$. The E_b / N_I required for $P_b = 10^{-5}$ when $E_b / N_0 = 10$ dB and $E_b / N_0 = 7.1$ dB for ρ=1, ρ=0.5 and ρ=0.1, respectively, are listed in Tables 4, 5 and 6. The results depicted in the plots and inserted into the tables are those that yield the best performance in each case under investigation. This is not true for the actual JTIDS waveforms because they have been included for comparison purposes.

36

From Figures 24, 25 and 26, we see that for $E_b / N_0 = 7.1$ dB, which leads asymptotically to $P_b = 10^{-6}$ for noncoherent demodulation, the E_b / N_I required for $P_b = 10^{-5}$ increases as ρ decreases for $\rho \geq 0.1$. Additionally, for $E_b / N_0 = 10$ dB and $P_b = 10^{-5}$, as ρ decreases, the difference in performance between the best waveforms for coherent and noncoherent demodulation increases from 1.6 dB to 2.3 dB when $\rho = 0.5$. For $\rho \leq 0.1$ and for $P_b = 10^{-5}$, both the coherent and noncoherent waveforms are not affected by the interference because they yield performance superior to $P_b = 10^{-5}$. Note that a reduction of E_b / N_0 requires an increase in E_b / N_I in order to maintain $P_b = 10^{-5}$. In the case of noncoherent detection, an approximately 3 dB decrease of E_b / N_0 leads to a greater than 3 dB increase in required E_b / N_I. The increase is more extreme for BNI, where E_b / N_I must increase by 10 dB. In the case of coherent detection, an approximately 3 dB decrease of E_b / N_0 leads to a greater than 3 dB increase in required E_b / N_I. The increase is more extreme for BNI, where E_b / N_I must increase by 13 dB. For both coherent and noncoherent demodulation, as ρ decreases, we note an increase in the required E_b / N_I. This is not the case when $\rho \leq 0.1$, in which case the performance of the alternative waveforms is better than $P_b = 10^{-5}$. We also note that the performance of the alternative waveform is always superior to that of the original JTIDS. Finally, we should note that for the case of coherent demodulation the best performance is achieved by the alternative waveform that uses a RS (31, 23) code as an inner code, whereas for the case of noncoherent reception, the best performance is given by the alternative waveform that uses the RS (31, 27) code as an inner code. Hence, superior throughput is obtained with noncoherent detection.
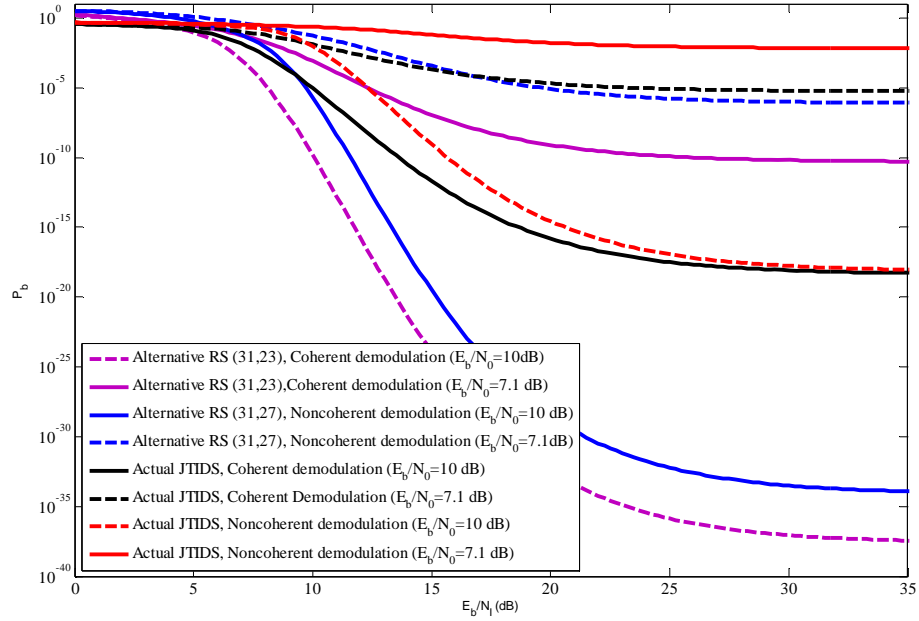
Figure 24.   Comparison of the performance of the alternative waveform with both AWGN and PNI for coherent and noncoherent demodulation and for $\rho=1$.

Table 4.   Comparison of the performance of the alternative waveform with both AWGN and PNI for coherent and noncoherent demodulation, hard decision decoding, $\rho=1$ and $P_b = 10^{-5}$ dB.

E_b / N_0 (dB)	Demodulation	Waveform	E_b / N_I (dB)
10	Coherent	Alternative RS (31,23)	8
10	Noncoherent	Alternative RS (31,27)	9.6
10	Coherent	Actual JTIDS	10
7.1	Coherent	Coherent RS (31,23)	12.2
10	Noncoherent	Actual JTIDS	12.2
7.1	Noncoherent	Alternative RS (31,27)	19.5
7.1	Coherent	Actual JTIDS	23
7.1	Noncoherent	Actual JTIDS	-

38
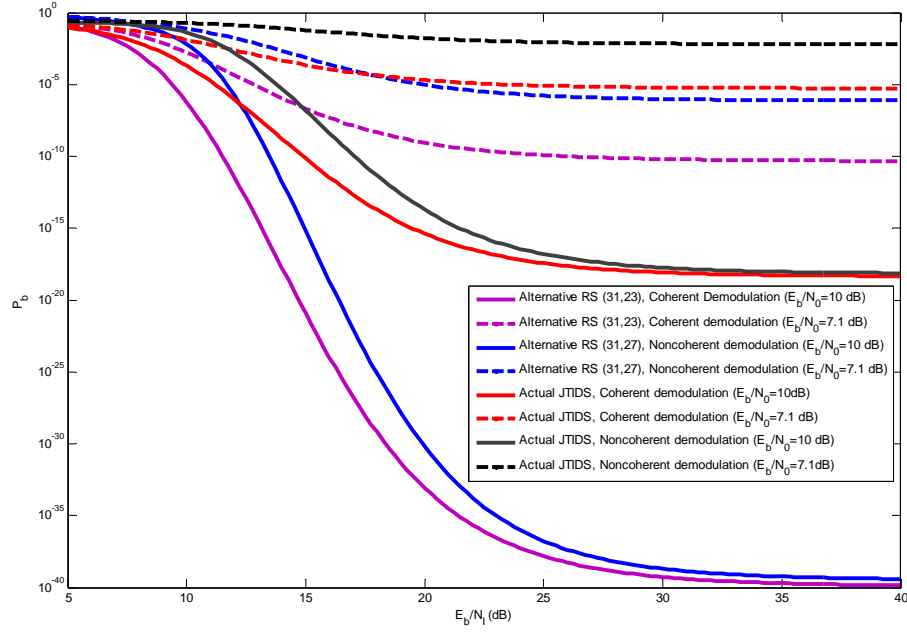
Figure 25.   Comparison of the performance of the alternative waveform with both AWGN and PNI for coherent and noncoherent demodulation and for ρ=0.5.

Table 5.   Comparison of the performance of the alternative waveform with both AWGN and PNI for coherent and noncoherent demodulation, hard decision decoding, ρ=0.5 and $P_b = 10^{-5}$ dB.

E_b / N_0 (dB)	Demodulation	Waveform	E_b / N_I (dB)
10	Coherent	Alternative RS (31,23)	9.4
10	Coherent	Actual JTIDS	11.1
10	Noncoherent	Alternative RS (31,27)	11.7
7.1	Coherent	Alternative RS (31,23)	12.7
10	Noncoherent	Actual JTIDS	13.7
7.1	Noncoherent	Alternative RS (31,27)	20
7.1	Coherent	Actual JTIDS	23.7
7.1	Noncoherent	Actual JTIDS	-
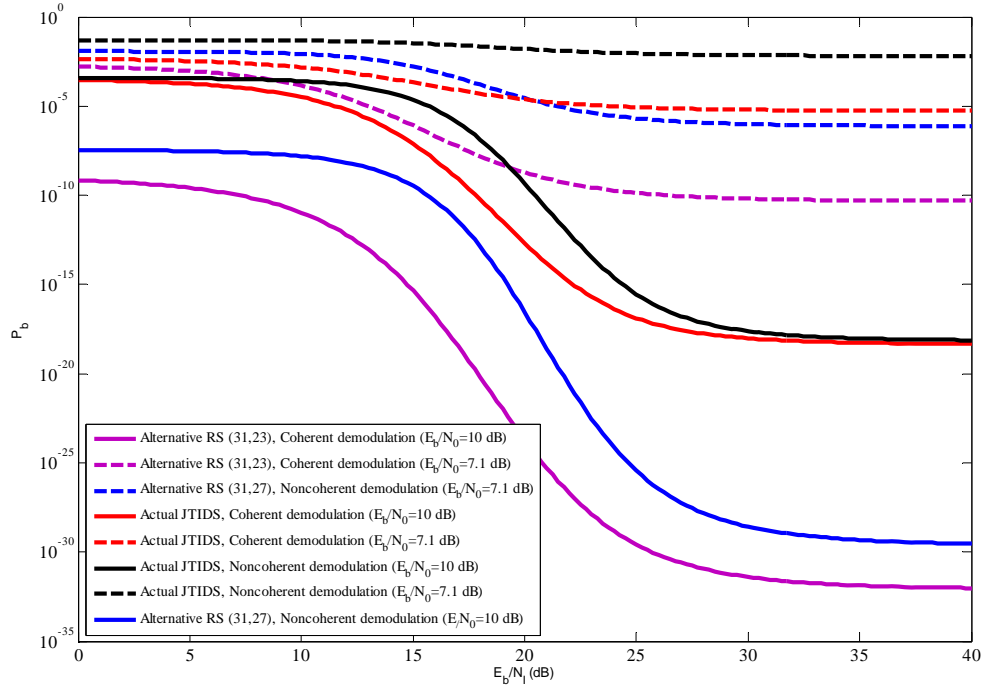
Figure 26.   Comparison of the performance of the alternative waveform with both AWGN and PNI for coherent and noncoherent demodulation and for $\rho=0.1$.

Table 6.   Comparison of the performance of the alternative waveform with both AWGN and PNI for coherent and noncoherent demodulation, hard decision decoding, $\rho=0.1$ and $P_b = 10^{-5}$ dB.

E_b / N_0 (dB)	Demodulation	Waveform	E_b / N_I (dB)
10	Coherent	Alternative RS (31,23)	0
10	Noncoherent	Alternative RS (31,27)	0
10	Coherent	Actual JTIDS	9.9
7.1	Coherent	Alternative RS (31,23)	13
10	Noncoherent	Actual JTIDS	15.6
7.1	Noncoherent	Alternative RS (31,27)	21.1
7.1	Coherent	Actual JTIDS	22.6
7.1	Noncoherent	Actual JTIDS	-

40

D. CHAPTER SUMMARY

In this chapter, the effects of AWGN and PNI on the performance of the alternative JTIDS waveform, for both coherent and noncoherent demodulation, were examined. In the next chapter, the performance analysis of coherent 32-ary CCSK with concatenated coding in an AWGN and PNI environment with a diversity of two will be examined. The performance of the alternative waveform is also compared to the original JTIDS waveform.

THIS PAGE INTENTIONALLY LEFT BLANK

V. PERFORMANCE ANALYSIS OF COHERENT 32-ARY CCSK WITH CONCATENATED CODING IN AN AWGN AND PULSED-NOISE INTERFERENCE ENVIRONMENT, WITH A DIVERSITY OF TWO

In this chapter, we examine the performance of coherent 32-*ary* CCSK with concatenated coding in an AWGN and pulse-noise interference environment with a diversity of two, which implies the double-pulse structure of JTIDS.

The double pulse-structure increases the anti-jam capability of the link because it provides a diversity of $L = 2$. The double-pulse symbol packet consists of two single pulses both modulated with the same channel symbol. The double-pulse has a duration of 26 microseconds. Although the two pulses contain identical information, the carrier frequencies for each are chosen independently. The double-pulse structure is illustrated in Figure 27.
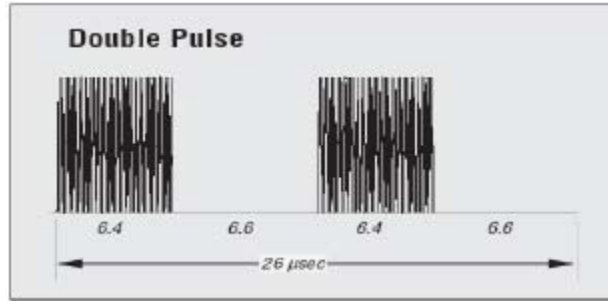
Figure 27. The standard JTIDS double-pulse structure [From 9])

A. PROBABILITY OF CHANNEL CHIP ERROR IN AWGN

When the double-pulse structure is used, JTIDS is a hybrid DS/fast frequency-hopping (FFH) spread spectrum system with sequential diversity $L = 2$ because each symbol is transmitted twice on different carrier frequencies. In this case, the average energy per symbol is [4]

$$E_S = LE_p, \tag{5.1}$$

where E_p is the average energy per pulse. Because $E_S = 5E_b$ and $E_p = 5E_{b'}$, from Equation (5.1) we get

$$E_b = LE_{b'}, \tag{5.2}$$

43

where $E_{b'}$ is the average energy per bit per pulse. Note that for a single-pulse, $E_b = E_{b'}$ because $L = 1$. Substituting Equation (5.2) into (3.6), we obtain a general expression for the probability of channel chip error of a Link-16/JTIDS-type waveform in AWGN as

$$p_c = Q\left(\sqrt{\frac{10rLE_{b'}}{32N_0}}\right),$$ (5.3)

where r is the code rate, $L = 1$ for the single-pulse structure, and $L = 2$ for the double-pulse structure.

B.   PERFORMANCE IN BOTH AWGN AND PNI

When a Link-16/JTIDS-type waveform is subjected to both AWGN and PNI, Equation (3.13) can still be used to evaluate the probability of bit error since Equation (3.13) is independent of the types of noise and/or fading channels; however, the probability of channel symbol error p_s shown in Equation (3.8) must be generalized as [4]

$$p_s = \sum_{l=0}^{L}\binom{L}{l}\rho^l(1-\rho)^{L-l}p_{s_l},$$ (5.4)

where $L = 1$ for the single-pulse structure, $L = 2$ for the double pulse structure, and p_{s_l} is the probability of channel symbol error given that l pulses are jammed and is upper-bounded by [4]

$$p_{s_l} < \sum_{j=0}^{32}\zeta_{UB_j}\binom{32}{j}p_{c_l}{}^j(1-p_{c_l})^{32-j},$$ (5.5)

where $l = 0,...,L$, and p_{c_l} is the probability of channel chip error given that l pulses are jammed. For coherent detection p_{c_l} is given by [4]

$$p_{c_l} = Q\left(\sqrt{\frac{0.3125rLE_{b'}}{N_0 + (lN_I / L\rho)}}\right).$$ (5.6)

44

C. COHERENT DEMODULATION OF 32-ARY CCSK WITH CONCATENATED CODING IN AN AWGN AND PNI ENVIRONMENT, WITH A DIVERSITY OF TWO

The probability of channel symbol error is given in general by Equation (5.4). Using $L = 2$ in Equation (5.4), we get

$$p_s = (1-\rho)^2 p_{s_0} + 2\rho(1-\rho) p_{s_1} + \rho^2 p_{s_2}, \tag{5.7}$$

where p_{s_0} is the probability of channel symbol error given that neither pulse is jammed, p_{s_1} is the probability of channel symbol error given that one pulse is jammed, and p_{s_2} is the probability of channel symbol error given that both pulses are jammed. From Equation (5.5), p_{s_0} is upper-bounded by

$$p_{s_0} < \sum_{j=0}^{32} \zeta_{UB_j} \binom{32}{j} p_{c_0}^{\ j} (1 - p_{c_0})^{32-j}, \tag{5.8}$$

and from Equation (5.6) with $l = 0$ and $L = 2$, p_{c_0} is given by

$$p_{c_0} = Q\left(\sqrt{\frac{0.3125 r E_b}{N_0}} \right). \tag{5.9}$$

Similarly, from Equation (5.5), p_{s_1} is upper-bounded by

$$p_{s_1} < \sum_{j=0}^{32} \zeta_{UB_j} \binom{32}{j} p_{c_1}^{\ j} (1 - p_{c_1})^{32-j}, \tag{5.10}$$

and from Equation (5.6) with $l = 1$ and $L = 2$, p_{c_1} is given by

$$p_{c_1} = Q\left(\sqrt{\frac{0.3125 r E_b}{N_0 + (N_I / 2\rho)}} \right). \tag{5.11}$$

From Equation (5.5), p_{s_2} is upper-bounded by

$$p_{s_2} < \sum_{j=0}^{32} \zeta_{UB_j} \binom{32}{j} p_{c_2}^{\ j} (1 - p_{c_2})^{32-j}, \tag{5.12}$$

and from Equation (5.6) with $l = 2$ and $L = 2$, p_{c_2} is given by

$$p_{c_2} = Q\left(\sqrt{\frac{0.3125 r E_b}{N_0 + N_I / \rho}} \right). \tag{5.13}$$

Now, using Equation (5.9) for different values of the concatenated code rate r in (5.8), we obtain the probability of channel symbol error given that neither pulse is jammed p_{s_0}. Using Equation (5.11) for different values of the concatenated code rate r in (5.10), we obtain the probability of channel symbol error given that one pulse is jammed p_{s_1}. Finally, using Equation (5.13) for different values of the concatenated code rate r in (5.12), we obtain the probability of channel symbol error given that both pulses are jammed p_{s_2}. Next, substituting p_{s_0}, p_{s_1} and p_{s_2} into Equation (5.7), we obtain the average probability of channel symbol error p_s. Using p_s in Equation (3.10), we obtain the probability of symbol error P_S at the output of the Reed-Solomon decoder. Next, using Equation (3.11) we obtain the probability of bit error p_b at the output of the symbol-to-bit converter. Finally, substituting p_b into Equation (3.12) and substituting Equation (3.12) into (3.13), we obtain the probability of bit error P_b of a Link-16/JTIDS-type system using the alternative error correction coding scheme for the physical layer, double-pulse structure, in both AWGN and PNI for coherent demodulation.

The performance of the alternative waveform as well as that of the existing Link-16/JTIDS for different values of ρ and different code rates r of the concatenated code for coherent demodulation of the double-pulse structure are shown in Figures 28–35. From the plots, we see that PNI degrades the performance of the system relative to barrage-noise interference $(\rho = 1)$ for $\rho > 0.1$. We also observe that the higher rate codes yield better performance for $\rho > 0.1$, whereas the lower rate codes give better results for $\rho \leq 0.1$ and for $E_b / N_0 > 8.4$ dB.

Figure 28.   Performance of 32-*ary* CCSK using concatenated coding in both
AWGN and PNI for ρ=1, coherent demodulation, $E_b / N_0 = 10$ dB and
diversity $L = 2$.

From Table 7, we can see that PNI degrades the performance of the alternative
system relative to barrage-noise interference ($\rho = 1$) when $P_b = 10^{-5}$ and for $\rho > 0.1$ by
0.8 dB, whereas the actual JTIDS performance is degraded by 0.6 dB. Nevertheless, the
absolute performance of the alternative waveform for $P_b = 10^{-5}$ is better compared to
that of the actual JTIDS by about 2 dB. We should note that the table entries are the
alternative waveforms that yield the best performance for each case under investigation.
For $\rho < 0.1$ and $E_b / N_0 = 10$ dB, the performance of the alternative waveform is not
affected for $P_b \geq 10^{-5}$, while actual JTIDS performance is not affected for $P_b \geq 10^{-5}$ and

$E_b / N_0 = 10$ dB when $\rho < 0.1$. Also, we observe that in each case the performance of the alternative waveform is superior to that of the original JTIDS. Indeed, that superiority becomes more dominant for $\rho \leq 0.1$.

Table 7. Performance of 32-*ary* CCSK with concatenated coding for different values of ρ in both AWGN and PNI for coherent demodulation, hard decision decoding, diversity $L = 2$ and $E_b / N_0 = 10$ dB.

P_b	ρ	Waveform	E_b / N_I **(dB)** (Existing JTIDS)	E_b / N_I **(dB)** (Alternative Waveform)
10^{-5}	1	Alternative RS(31,23)	10	8
10^{-5}	0.5	Alternative RS(31,23)	10.6	8.8
10^{-5}	0.1	Alternative RS(31,11)	12.2	4.4

Figure 29. Performance of 32-*ary* CCSK using concatenated coding in both AWGN and PNI for $\rho=1$, coherent demodulation, $E_b / N_0 = 6.1$ dB and diversity $L = 2$.

48

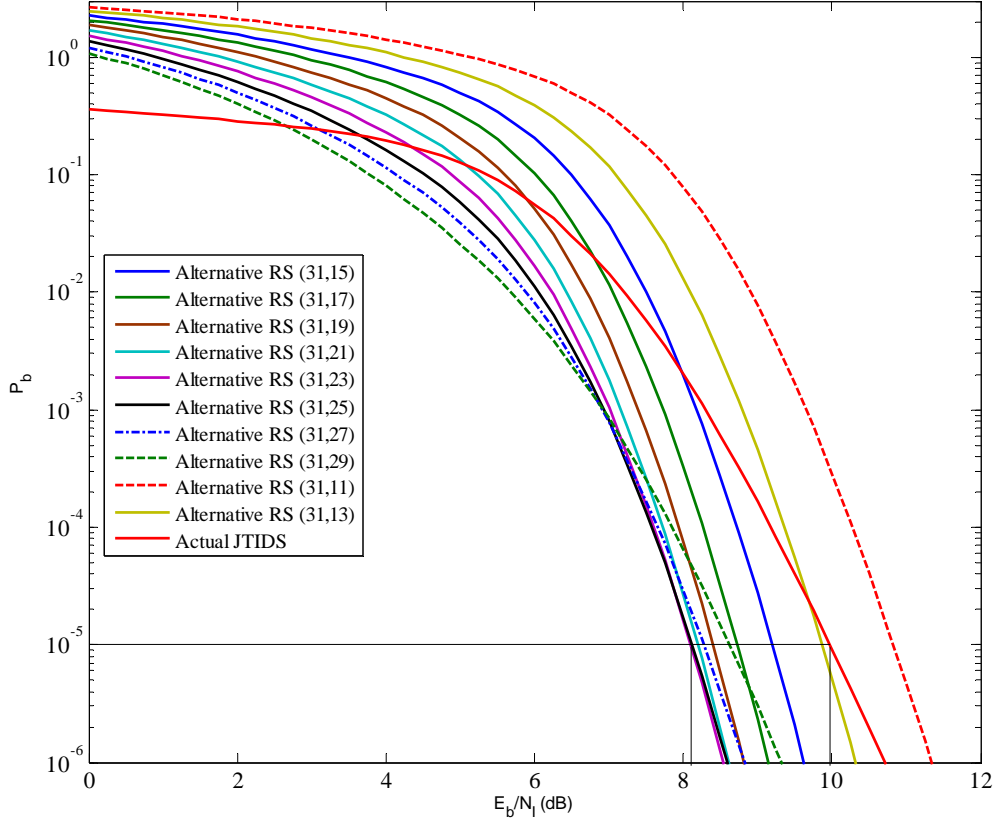Figure 30.   Performance of 32-*ary* CCSK using concatenated coding in both
AWGN and PNI for ρ=0.5, coherent demodulation, $E_b / N_0 = 10$ dB
and diversity $L = 2$.

We also notice from Figures 28 through 35 that the performance of both the Link-16/JTIDS-type waveform with the alternative error correction coding scheme for the physical layer and the actual JTIDS is not affected for $\rho < 0.1$ and for $E_b / N_I > 7.9$ dB, because in each case $P_b < 10^{-6}$.

49

Figure 31.   Performance of 32-*ary* CCSK using concatenated coding in both AWGN and PNI for ρ=0.5, coherent demodulation, $E_b / N_0 = 6.2$ dB and diversity $L = 2$.

Figure 32.   Performance of 32-*ary* CCSK using concatenated coding in both
AWGN and PNI for ρ=0.1, coherent demodulation, $E_b / N_0 = 10$ dB
and diversity $L = 2$.

51

Figure 33.   Performance of 32-*ary* CCSK using concatenated coding in both AWGN and PNI for ρ=0.1, coherent demodulation, $E_b / N_0 = 6.2$ dB and diversity $L = 2$.

Figure 34. Performance of 32-*ary* CCSK using concatenated coding in both AWGN and PNI for ρ=0.01, coherent demodulation, $E_b / N_0 = 10$ dB and diversity $L = 2$.
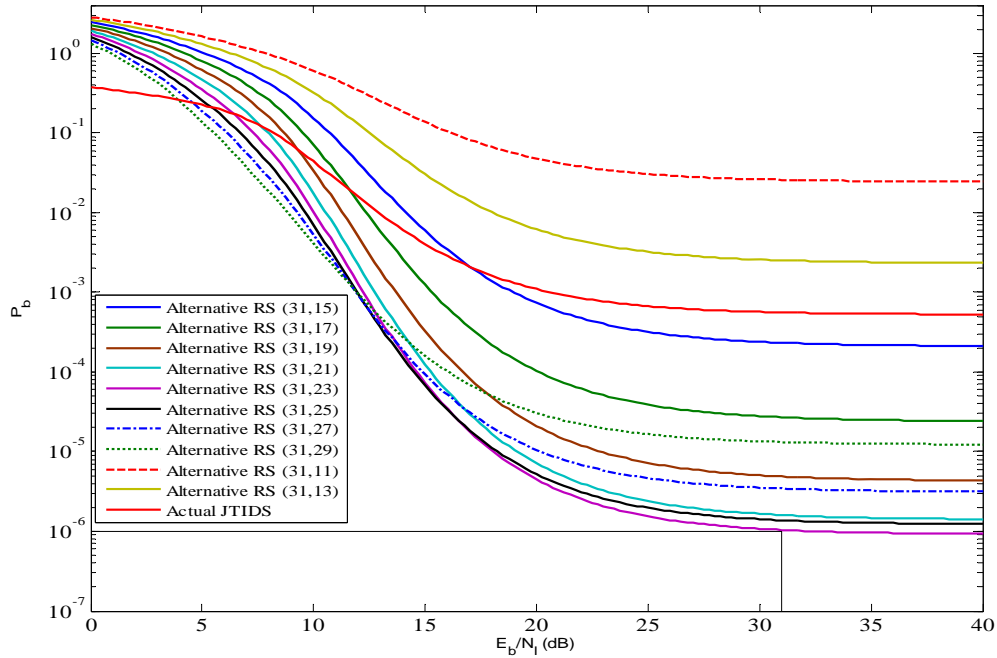
Figure 35.   Performance of 32-*ary* CCSK using concatenated coding in both AWGN and PNI for $\rho=0.01$, coherent demodulation, $E_b / N_0 = 6.2$ dB and diversity $L = 2$.
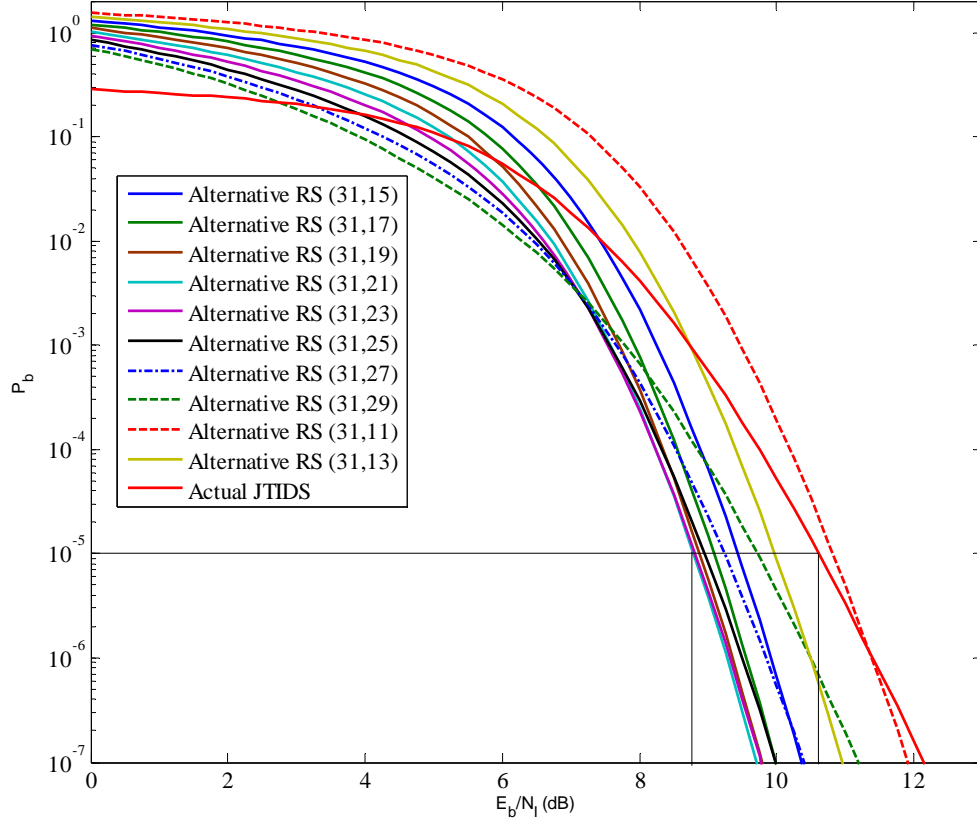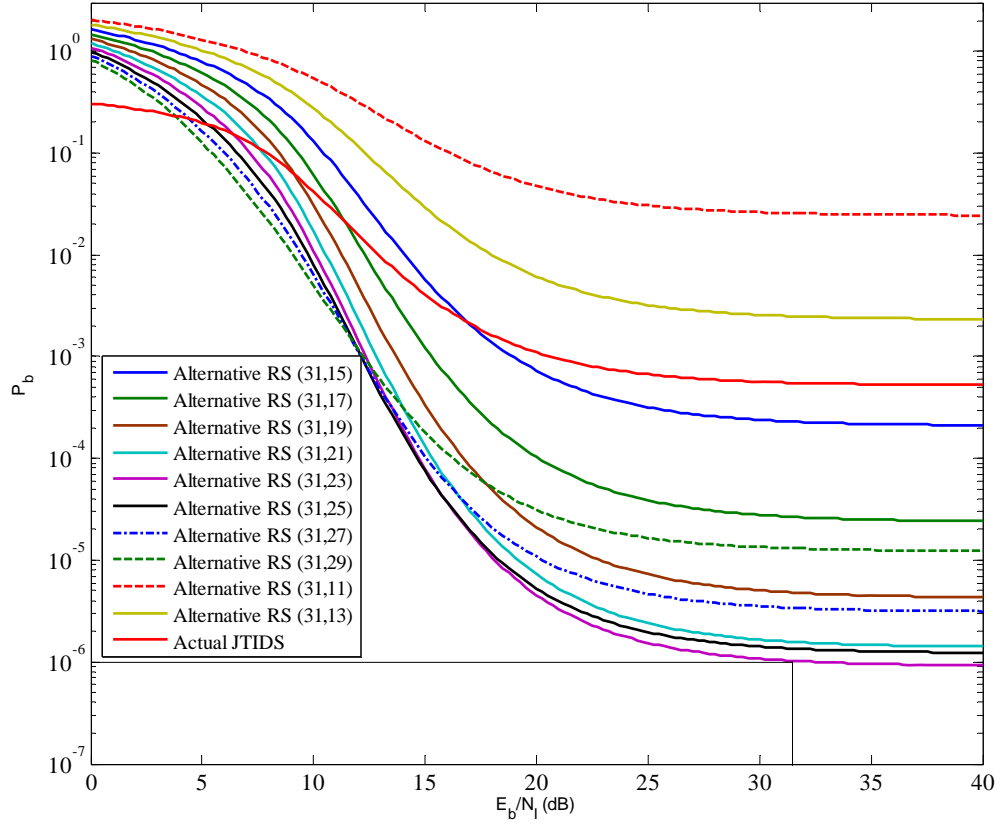
D.   COHERENT DEMODULATION OF 32-ARY CCSK WITH CONCATENATED CODING IN AN AWGN AND PNI ENVIRONMENT, WITH A DIVERSITY OF TWO AND PERFECT SIDE INFORMATION

In some cases, the system performance can be improved further if we have some information regarding which pulse is jammed and which is not. When available, this information is called side information. Perfect side information (PSI) is not realistic but gives us a benchmark against which to measure receivers that have imperfect or no side information. For PSI, we assume that the jammed pulse is disregarded except when all pulses are jammed. Given this assumption, PSI has no effect on the single-pulse structure but will affect the double-pulse structure because there is a possibility that one of the two pulses will experience jamming. With PSI, Equation (5.11) becomes

54

$$p_{c_1} = Q\left(\sqrt{\frac{0.3125rE_b}{N_0}}\right), \tag{5.14}$$

while p_{c_0} and p_{c_2}, shown in Equations (5.9) and (5.13), respectively, remain the same. Now, using Equation (5.9) for different values of the concatenated code rate r in (5.8), we obtain the probability of channel symbol error given that neither pulse is jammed p_{s_0}. Using Equation (5.14) for different values of the concatenated code rate r in (5.10), we obtain the probability of channel symbol error given that one pulse is jammed p_{s_1}. Finally, using Equation (5.13) for different values of the concatenated code rate r in (5.12), we obtain the probability of channel symbol error given that both pulses are jammed p_{s_2}. Next, substituting p_{s_0}, p_{s_1} and p_{s_2} into Equation (5.7), we obtain the average probability of channel symbol error p_s. Using p_s in Equation (3.10), we obtain the probability of symbol error P_S at the output of the Reed-Solomon decoder. Next, using Equation (3.11) we obtain the probability of bit error p_b at the output of the symbol-to-bit converter. Finally, substituting p_b into Equation (3.12) and substituting Equation (3.12) into (3.13), we obtain the probability of bit error P_b of a Link-16/JTIDS-type system using the alternative error correction coding scheme for the physical layer, double-pulse structure, in both AWGN and PNI for coherent demodulation and assuming perfect side information.

The performance of the alternative waveform, as well as the existing Link-16/JTIDS, assuming perfect side information (PSI) for different values of ρ and different code rates r of the concatenated code for coherent demodulation and diversity $L = 2$ are shown in Figures 36 through 43. From the plots, we see that PNI does not degrade the performance of the system relative to barrage-noise interference. We also observe that the higher rate codes yield better performance for $\rho > 0.5$, whereas the lower rate codes give better results for $\rho \leq 0.5$ and for $E_b / N_0 > 8.7$ dB.
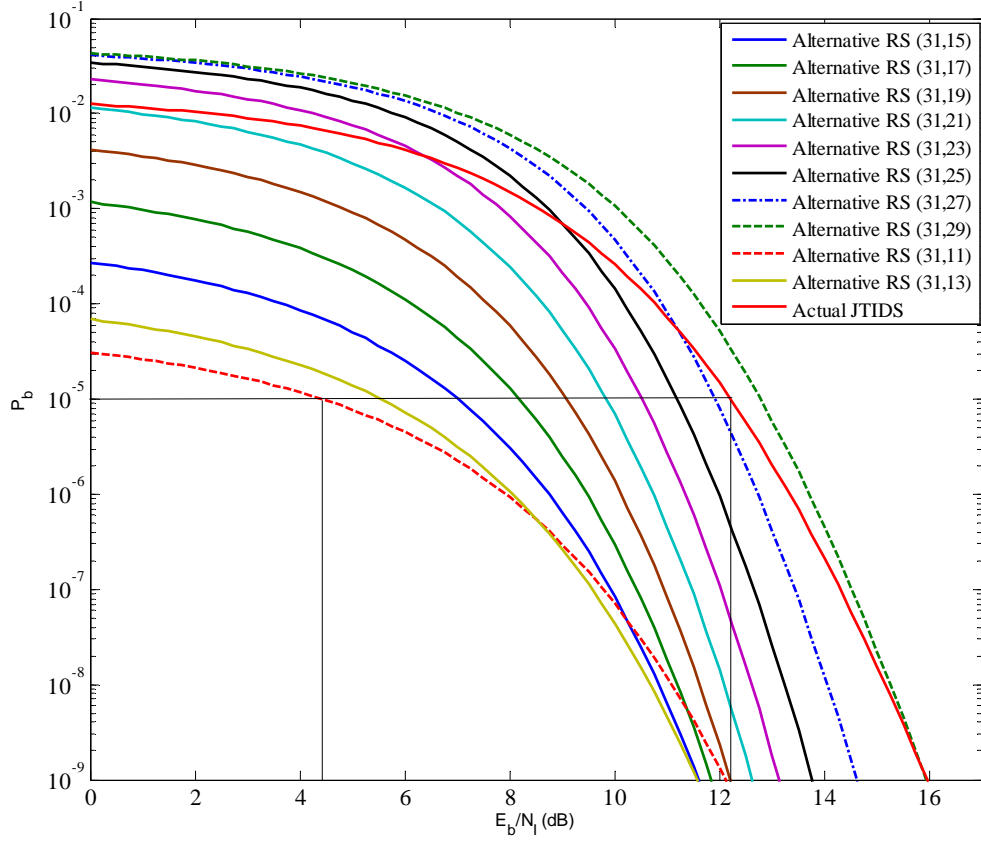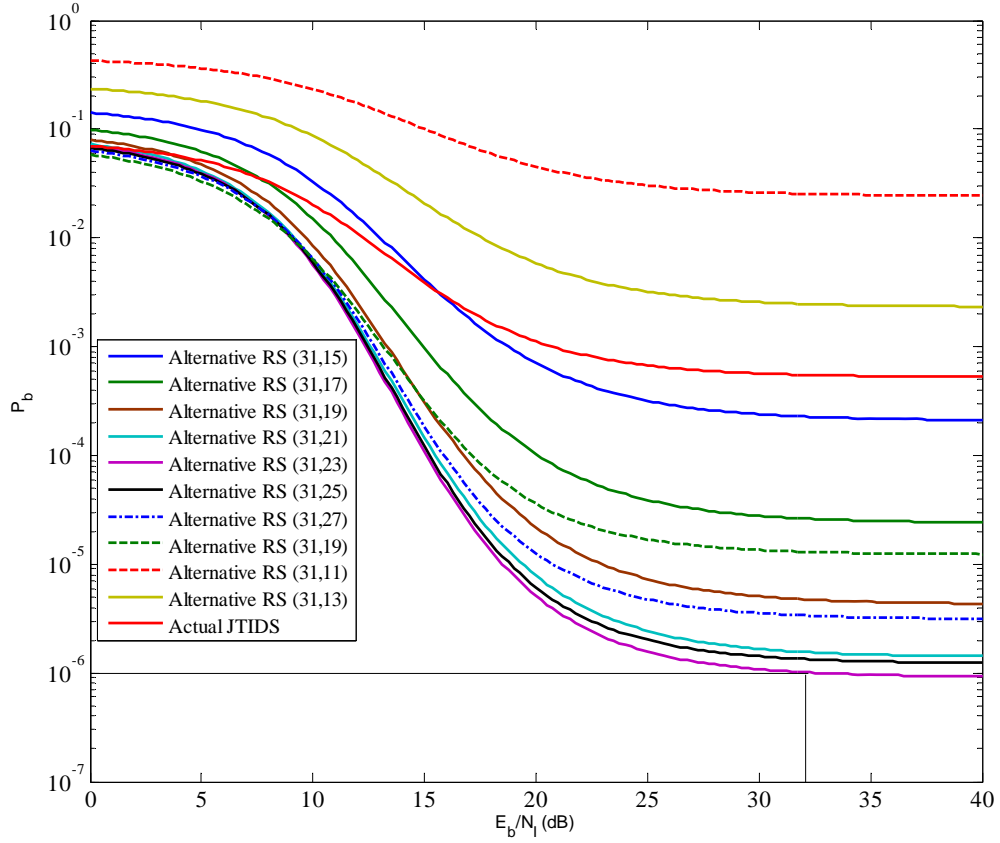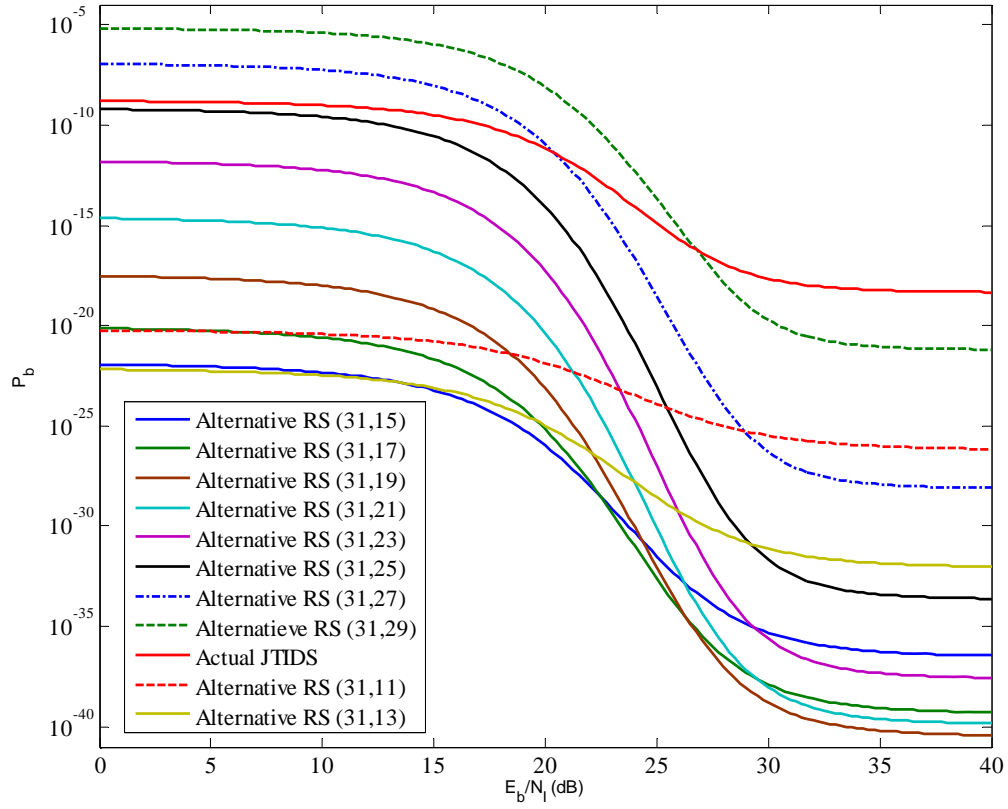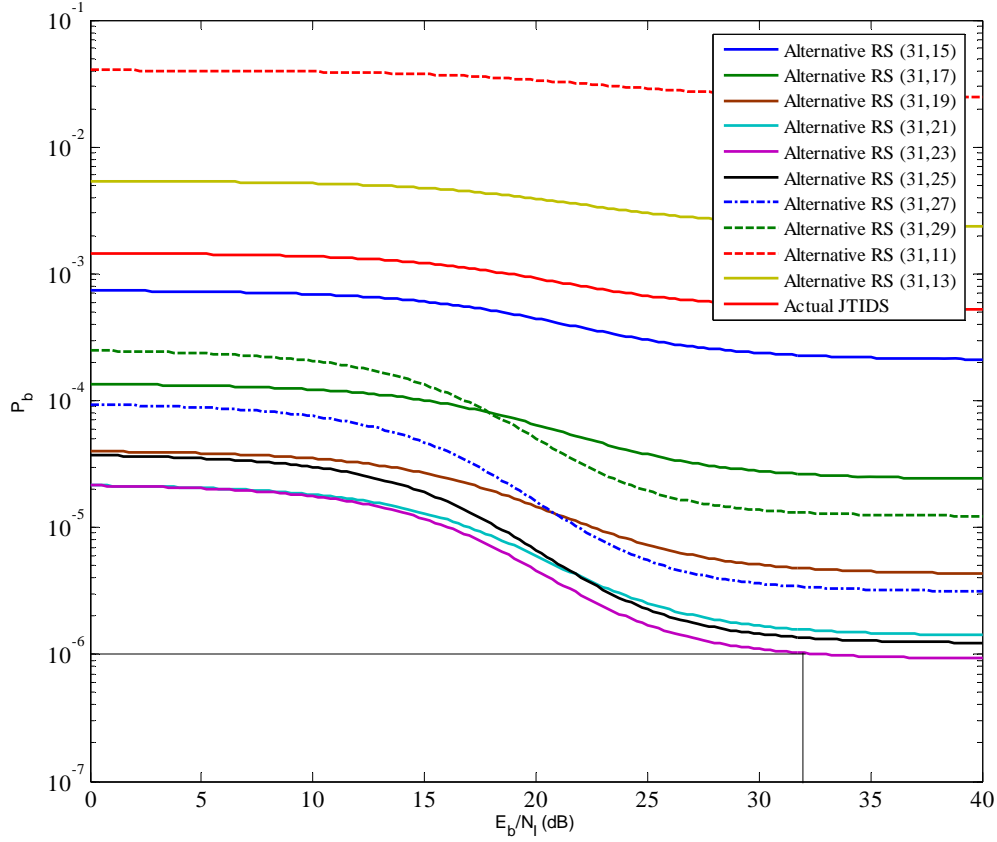
Figure 36.   Performance of 32-*ary* CCSK using concatenated coding in both AWGN and PNI for ρ=1, coherent demodulation, $E_b / N_0 = 10\,\text{dB}$, diversity $L = 2$, and PSI.

From Table 8, we can see that PNI does not degrade the performance of either the alternative system or the actual JTIDS relative to barrage-noise interference for $P_b = 10^{-5}$. We should note that table entries are for the alternative waveforms that yield the best performance for each case under investigation. For $\rho < 0.5$ and $E_b / N_0 = 10$ dB, the performance of the alternative waveform is not affected for $P_b \geq 10^{-5}$, while actual JTIDS performance is not affected for $P_b \geq 10^{-5}$ and $E_b / N_0 = 10$ dB when $\rho < 0.5$. We also observe that in each case the performance of the alternative waveform is superior to that of the actual JTIDS.

Table 8.   Performance of 32-*ary* CCSK with concatenated coding for different values of ρ in both AWGN and PNI for coherent demodulation, hard decision decoding, diversity $L = 2$, $E_b / N_0 = 10$ dB, and PSI.

P_b	ρ	**Waveform**	E_b / N_I **(dB)** **(Existing JTIDS)**	E_b / N_I **(dB)** **(Alternative Waveform)**
10^{-5}	1	Alternative RS(31,23)	10	8.1
10^{-5}	0.5	Alternative RS(31,13)	8.9	5.7

Figure 37.   Performance of 32-*ary* CCSK using concatenated coding in both AWGN and PNI for $\rho=1$, coherent demodulation, $E_b / N_0 = 6.2$ dB, diversity $L = 2$, and PSI.
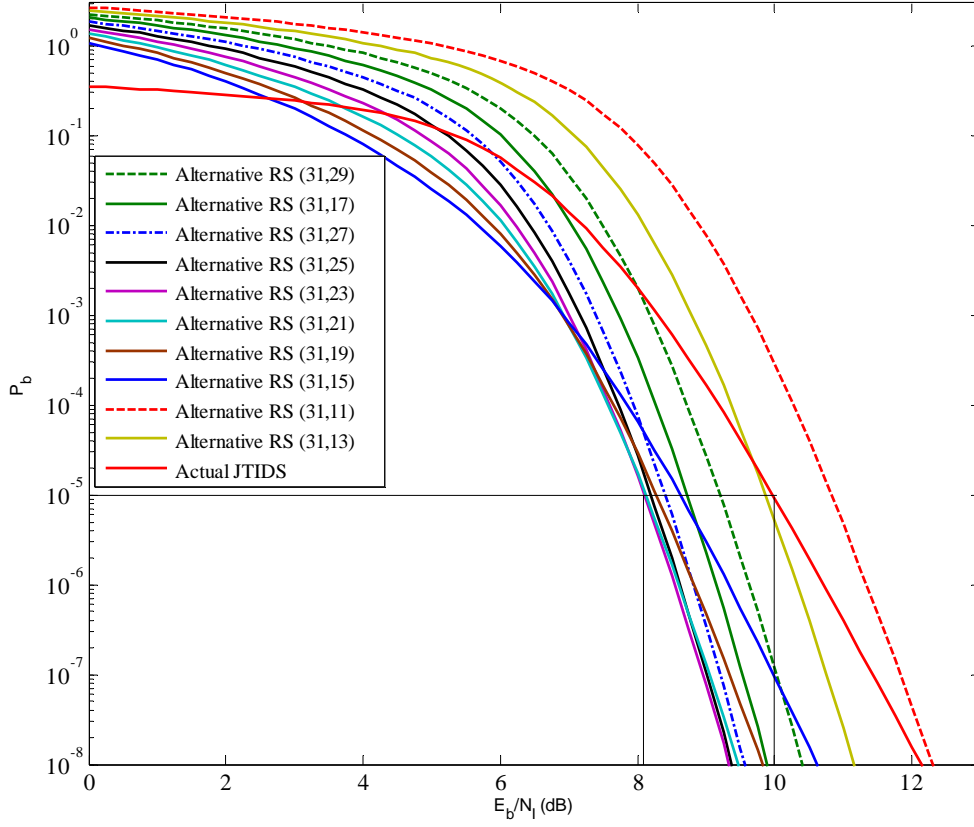
57
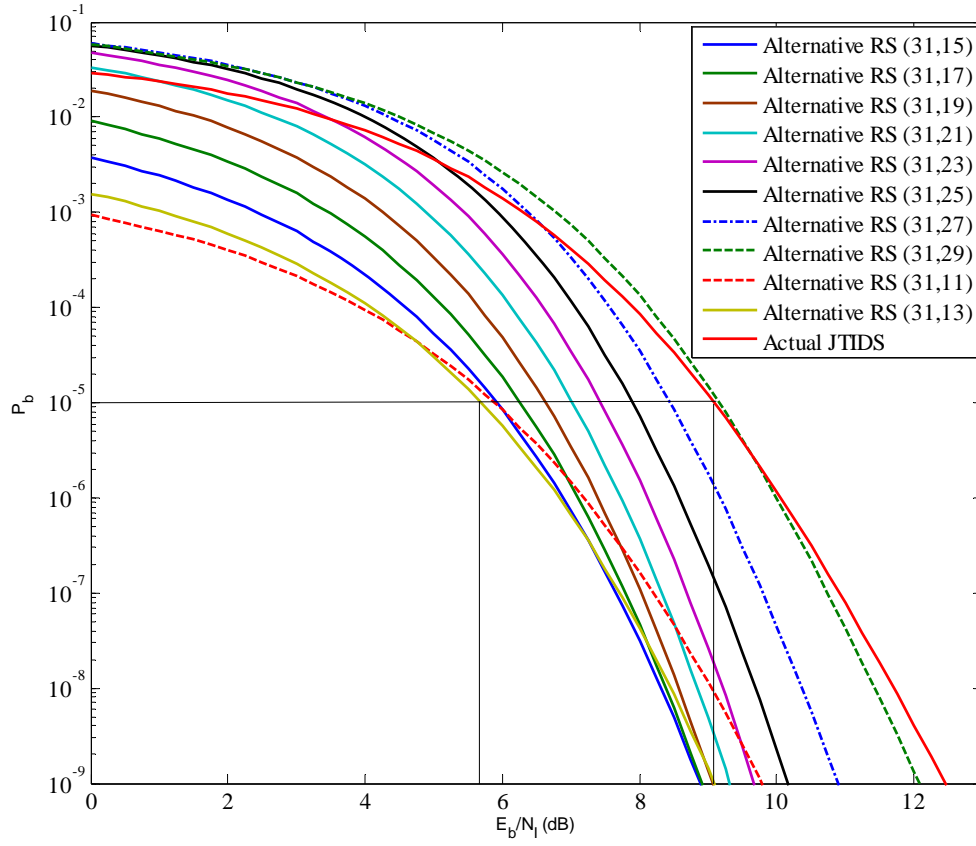
Figure 38. Performance of 32-*ary* CCSK using concatenated coding in both AWGN and PNI for $\rho=0.5$, coherent demodulation, $E_b / N_0 = 10$ dB, diversity $L = 2$, and PSI.

We should also notice from the Figures 36 through 43 that the performance of both the Link-16/JTIDS-type waveform with the alternative error correction coding scheme for the physical layer and the actual JTIDS is not affected for $\rho \leq 0.1$ when $E_b / N_I > 7.8$ dB since $P_b < 10^{-6}$.
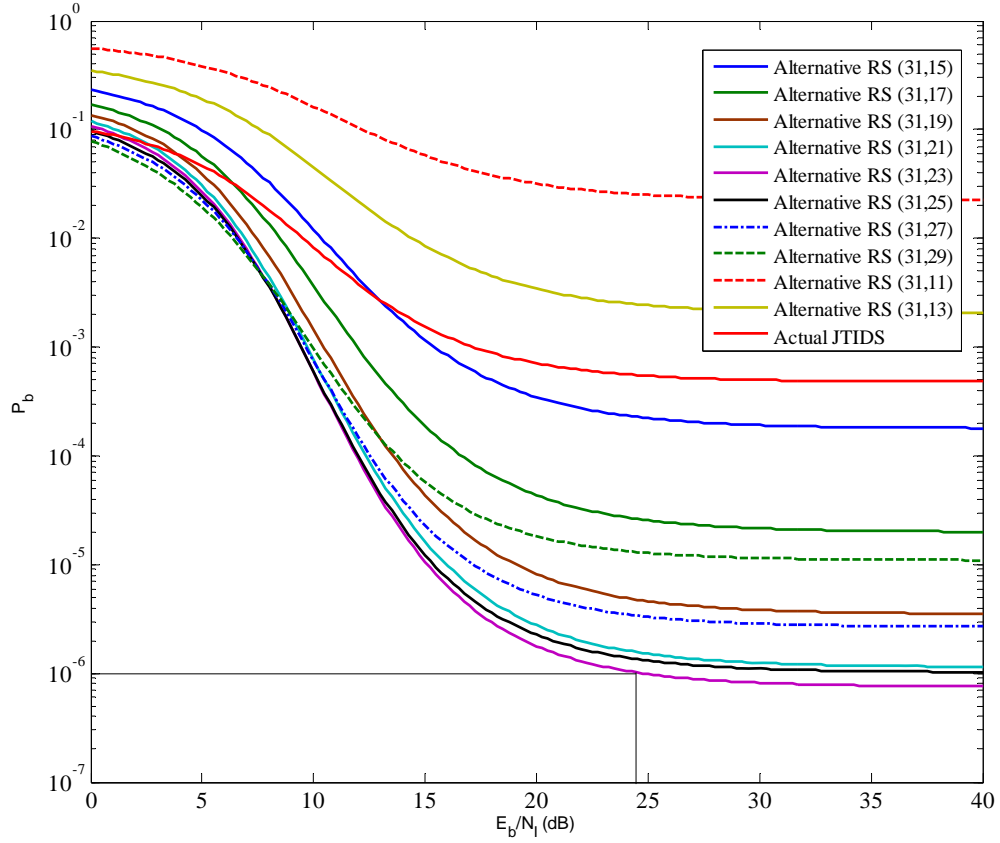
Figure 39.   Performance of 32-*ary* CCSK using concatenated coding in both
AWGN and PNI for ρ=0.5, coherent demodulation, $E_b / N_0 = 6.2$ dB,
diversity $L = 2$, and PSI.

Figure 40. Performance of 32-*ary* CCSK using concatenated coding in both AWGN and PNI for $\rho=0.1$, coherent demodulation, $E_b / N_0 = 10$ dB, diversity $L = 2$, and PSI.
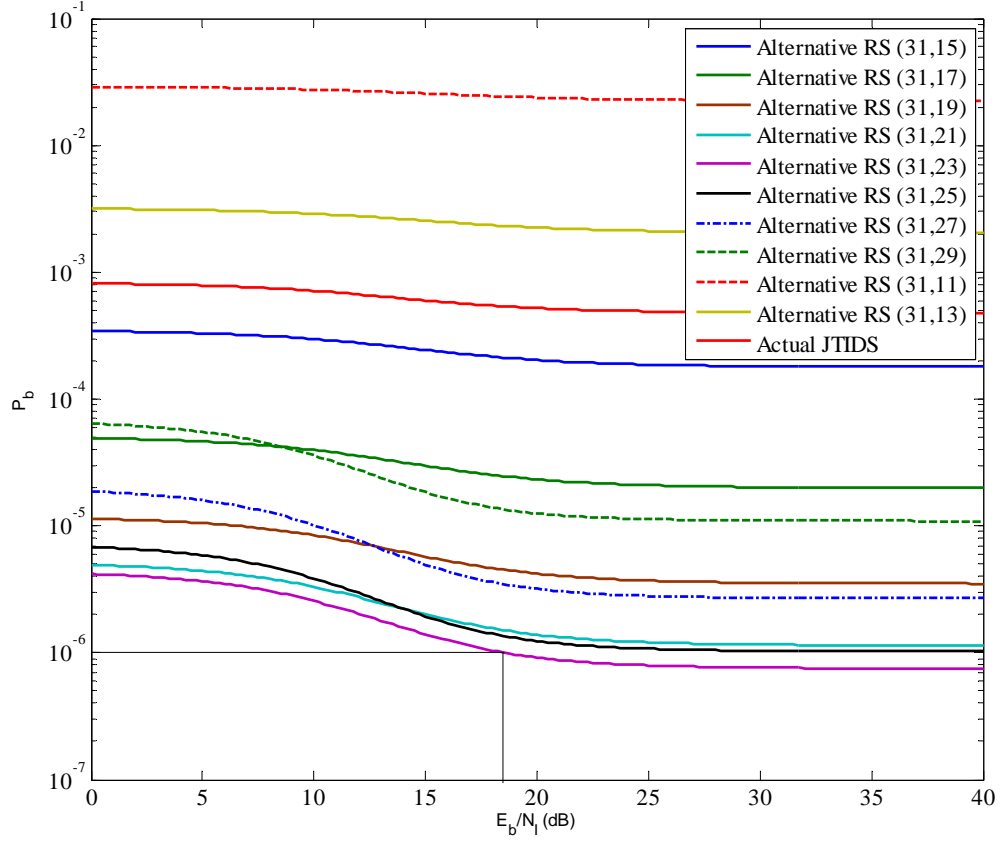
Figure 41.   Performance of 32-*ary* CCSK using concatenated coding in both AWGN and PNI for ρ=0.1, coherent demodulation, $E_b / N_0 = 6.2$ dB, diversity $L = 2$, and PSI.
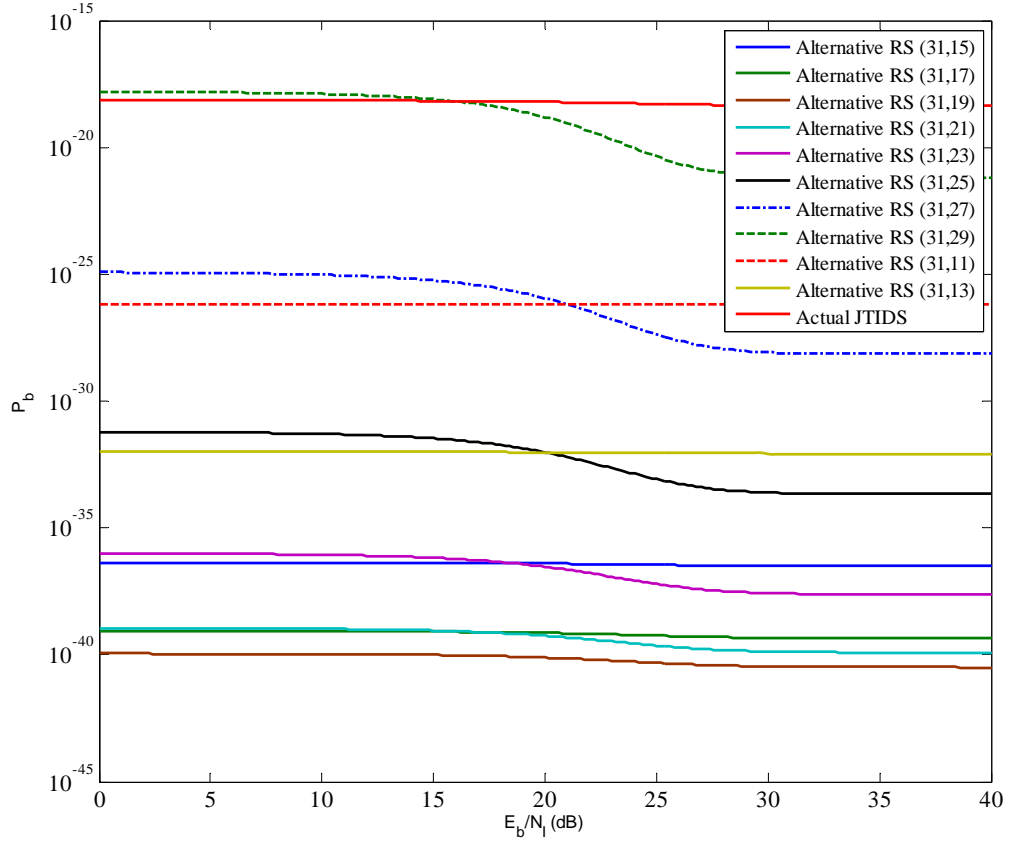
Figure 42.   Performance of 32-*ary* CCSK using concatenated coding in both AWGN and PNI for ρ=0.01, coherent demodulation, $E_b / N_0 = 10$ dB, diversity $L = 2,$ and PSI.
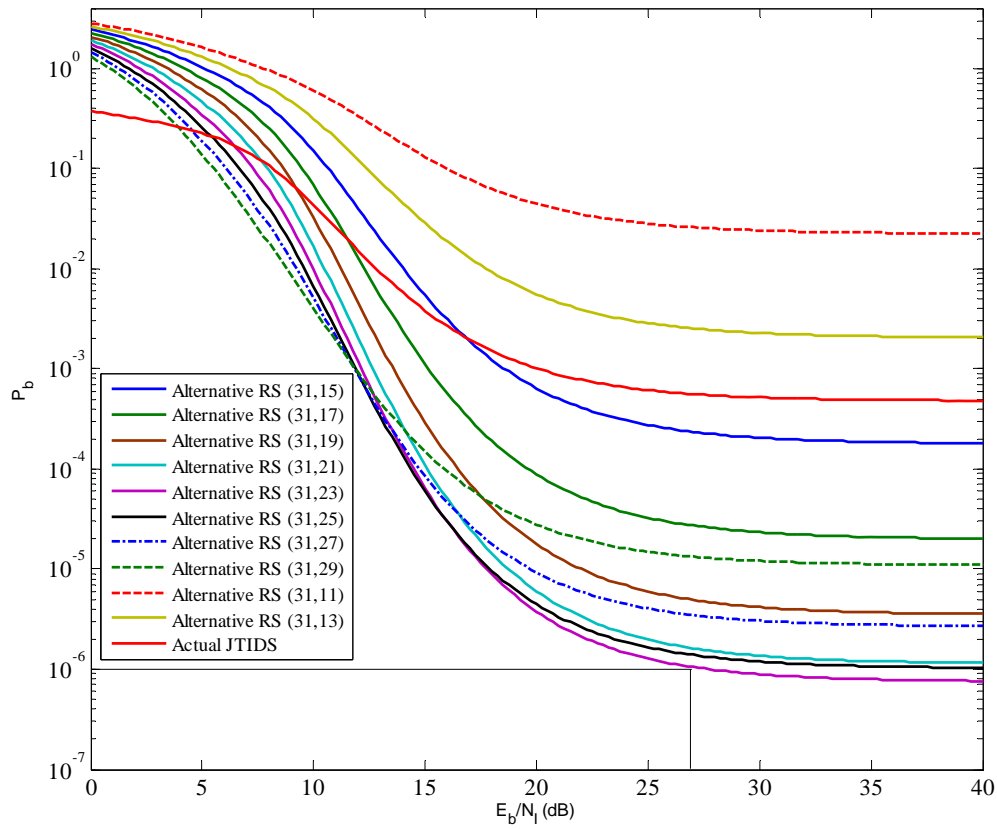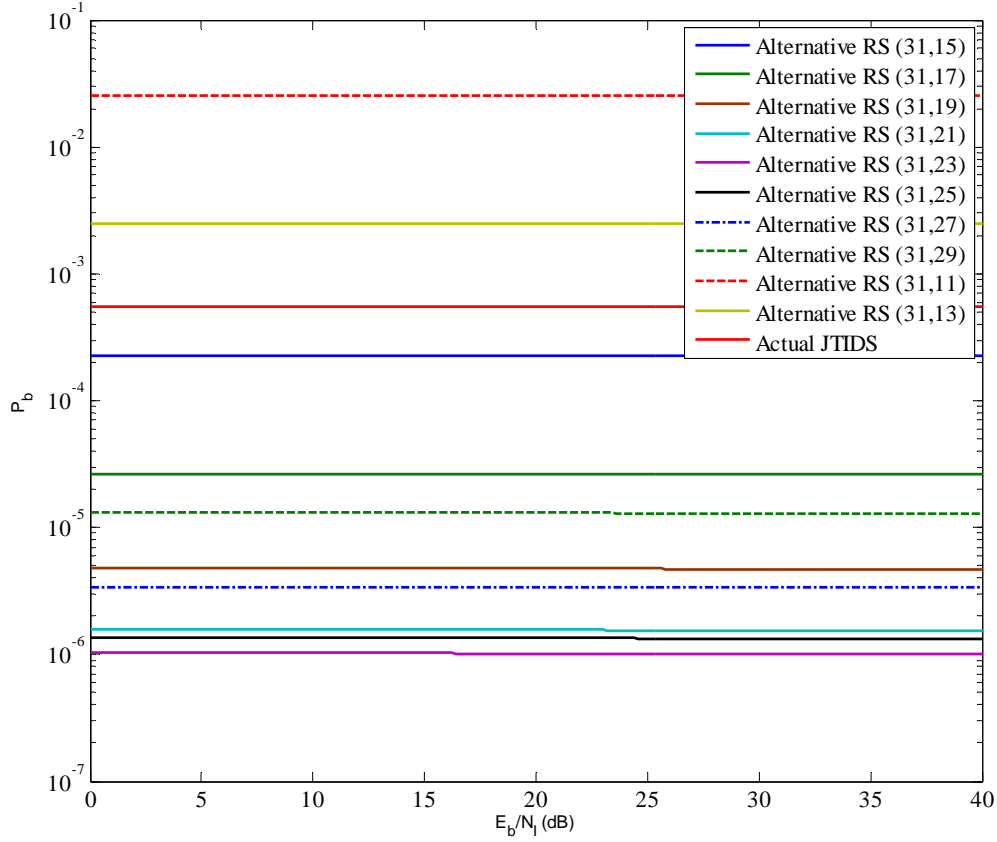
Figure 43.   Performance of 32-*ary* CCSK using concatenated coding in both AWGN and PNI for ρ=0.01, coherent demodulation, $E_b / N_0 = 6.2$ dB, diversity $L = 2$, and PSI.

E.   CHAPTER SUMMARY

In this chapter, the effects of AWGN and PNI on the performance of the alternative JTIDS waveform with a diversity of two for coherent demodulation were examined. In the next chapter, the performance analysis of noncoherent 32-ary CCSK with concatenated coding in an AWGN and PNI environment with a diversity of two with perfect side information will be examined. The performance of the alternative waveform is also compared to the original JTIDS waveform.

THIS PAGE INTENTIONALLY LEFT BLANK

VI. PERFORMANCE ANALYSIS OF NONCOHERENT 32-ARY CCSK WITH CONCATENATED CODING IN AN AWGN AND PULSED-NOISE INTERFERENCE ENVIRONMENT, WITH A DIVERSITY OF TWO AND PERFECT SIDE INFORMATION

In this chapter, we examine the performance of noncoherent 32-*ary* CCSK with concatenated coding in an AWGN and pulsed-noise interference environment with a diversity of two, which implies the double-pulse structure of JTIDS, assuming perfect side information (PSI).

A. NONCOHERENT DEMODULATION OF 32-ARY CCSK WITH CONCATENATED CODING IN AN AWGN AND PNI ENVIRONMENT, WITH A DIVERSITY OF TWO AND PSI

The probability of channel symbol error is given in general by Equation (5.4). Now, using $L = 2$ in Equation (5.4), we get

$$p_s = (1-\rho)^2 p_{s_0} + 2\rho(1-\rho)p_{s_1} + \rho^2 p_{s_2},\qquad(6.1)$$

where p_{s_0} is the probability of channel symbol error given that neither pulse is jammed, p_{s_1} is the probability of channel symbol error given that one pulse is jammed, and p_{s_2} is the probability of channel symbol error given that both pulses are jammed. From Equation (5.5), p_{s_0} is upper-bounded by

$$p_{s_0} < \sum_{j=0}^{32} \zeta_{UB_j} \binom{32}{j} p_{c_0}^{\ j}(1-p_{c_0})^{32-j}.\qquad(6.2)$$

The probability of chip error p_{c_0} when neither pulse is jammed is given by [11]

$$p_{c_0} = \frac{1}{2^{2L-1}}\exp\left(\frac{-LE_C}{N_0}\right)\sum_{n=0}^{L-1}c_n\left(\frac{LE_C}{N_0}\right)^n,\qquad(6.3)$$

where c_n is given by [11]

$$c_n = \frac{1}{n!}\sum_{m=0}^{L-1-n}\binom{2L-1}{m},\qquad(6.4)$$

and E_C is the average signal energy per diversity reception. Now taking into account Equation (3.14) and the fact that FEC is used, Equation (6.3) becomes

$$p_{c_0} = \frac{1}{2^{2L-1}} \exp\left(\frac{-0.3125 rLE_{b'}}{N_0}\right) \sum_{n=0}^{L-1} c_n \left(\frac{0.3125 rLE_{b'}}{N_0}\right)^n. \tag{6.5}$$

Using Equation (5.2) in Equation (6.5), we get

$$p_{c_0} = \frac{1}{2^{2L-1}} \exp\left(\frac{-0.3125 rE_b}{N_0}\right) \sum_{n=0}^{L-1} c_n \left(\frac{0.3125 rE_b}{N_0}\right)^n. \tag{6.6}$$

Similarly, from Equation (5.5), p_{s_1} is upper-bounded by

$$p_{s_1} < \sum_{j=0}^{32} \zeta_{UB_j} \binom{32}{j} p_{c_1}{}^j (1 - p_{c_1})^{32-j}, \tag{6.7}$$

where p_{c_1} is the probability of channel chip error when one out of the two pulses is jammed and is given by Equation (4.9) when PSI is available, which is reproduced here for convenience:

$$p_{c_1} = \frac{1}{2} \exp(-10 rE_b / 32 N_0). \tag{6.8}$$

From Equation (5.5), p_{s_2} is upper-bounded by

$$p_{s_2} < \sum_{j=0}^{32} \zeta_{UB_j} \binom{32}{j} p_{c_2}{}^j (1 - p_{c_2})^{32-j}, \tag{6.9}$$

and the probability of channel chip error when both pulses are jammed is given by

$$p_{c_2} = \frac{1}{2^{2L-1}} \exp\left(\frac{-0.3125 rE_b}{N_0 + N_I / \rho}\right) \sum_{n=0}^{L-1} c_n \left(\frac{0.3125 rE_b}{N_0 + N_I / \rho}\right)^n. \tag{6.10}$$

Now, using Equation (6.6) for different values of the concatenated code rate r in (6.2), we obtain the probability of channel symbol error given that neither pulse is jammed p_{s_0}. Using Equation (6.8) for different values of the concatenated code rate r in (6.7), we obtain the probability of channel symbol error given that one pulse is jammed p_{s_1}. Finally, using Equation (6.10) for different values of the concatenated code rate r in (6.9), we obtain the probability of channel symbol error given that both pulses are jammed p_{s_2}. Next, substituting p_{s_0}, p_{s_1} and p_{s_2} into Equation (6.1), we obtain the average probability of channel symbol error p_s. Substituting p_s into Equation (3.10), we obtain the probability of symbol error P_S at the output of the Reed-Solomon decoder.

Next, using Equation (3.11), we obtain the probability of bit error p_b at the output of the symbol-to-bit converter. Finally, substituting the bit error probability p_b in Equation (3.12) and substituting Equation (3.12) into (3.13), we obtain the probability of bit error P_b of a Link-16/JTIDS-type system using the alternative error correction coding scheme for the physical layer, double-pulse structure, in both AWGN and PNI, for noncoherent demodulation and assuming perfect side information. The results are shown in Figures 44 through 51. From the plots, we see that PNI degrades the performance of the system relative to BNI ($\rho = 1$) for $\rho \geq 0.5$. We also observe that the higher rate codes yield better performance for higher values of E_b / N_0, whereas smaller rate codes yield better performance for small values of E_b / N_0.

From Table 9 we can see that PNI degrades the performance of the alternative system relative to BNI when $P_b = 10^{-5}$ by 0.1 dB, whereas the performance of the actual JTIDS remains very poor regardless the value of ρ. We should note that the table entries are the alternative waveforms that yield the best performance for each case under investigation. For $\rho \leq 0.1$, and $E_b / N_0 = 10$ dB, the performance of the alternative waveform is not affected for $P_b = 10^{-5}$, while actual JTIDS performance remains poorer than $P_b = 10^{-5}$ regardless the value of ρ. Also, we observe that in each case the performance of the alternative waveform is superior to that of the original JTIDS.

Table 9. Performance of 32-*ary* CCSK with the concatenated code for different values of ρ in both AWGN and PNI for noncoherent demodulation, hard decision decoding, PSI, $L=2$ and $E_b/N_0 = 10$ dB.

P_b	ρ	Waveform	E_b/N_I (dB) (Existing JTIDS)	E_b/N_I (dB) (Alternative Waveform)
10^{-5}	1	Alternative RS(31,27)	>40	12.2
10^{-5}	0.5	Alternative RS(31,21)	>40	12.3
10^{-5}	0.1	Alternative RS(31,19)	>40	0
10^{-5}	0.01	Alternative RS(31,23)	>40	0

Figure 44. Performance of 32-*ary* CCSK using concatenated coding in both AWGN and PNI for ρ=1, noncoherent demodulation, $E_b/N_0 = 10$ dB, diversity $L=2$ and PSI.

Figure 45.   Performance of 32-*ary* CCSK using concatenated coding in both AWGN and PNI for $\rho=1$, noncoherent demodulation, $E_b / N_0 = 8.2$ dB, diversity $L = 2$ and PSI.

Figure 46. Performance of 32-*ary* CCSK using concatenated coding in both AWGN and PNI for $\rho=0.5$, noncoherent demodulation, $E_b/N_0 = 10$ dB, diversity $L = 2$ and PSI.

Figure 47.   Performance of 32-*ary* CCSK using concatenated coding in both AWGN and PNI for $\rho=0.5$, noncoherent demodulation, $E_b / N_0 = 7.8$ dB, diversity $L = 2$ and PSI.
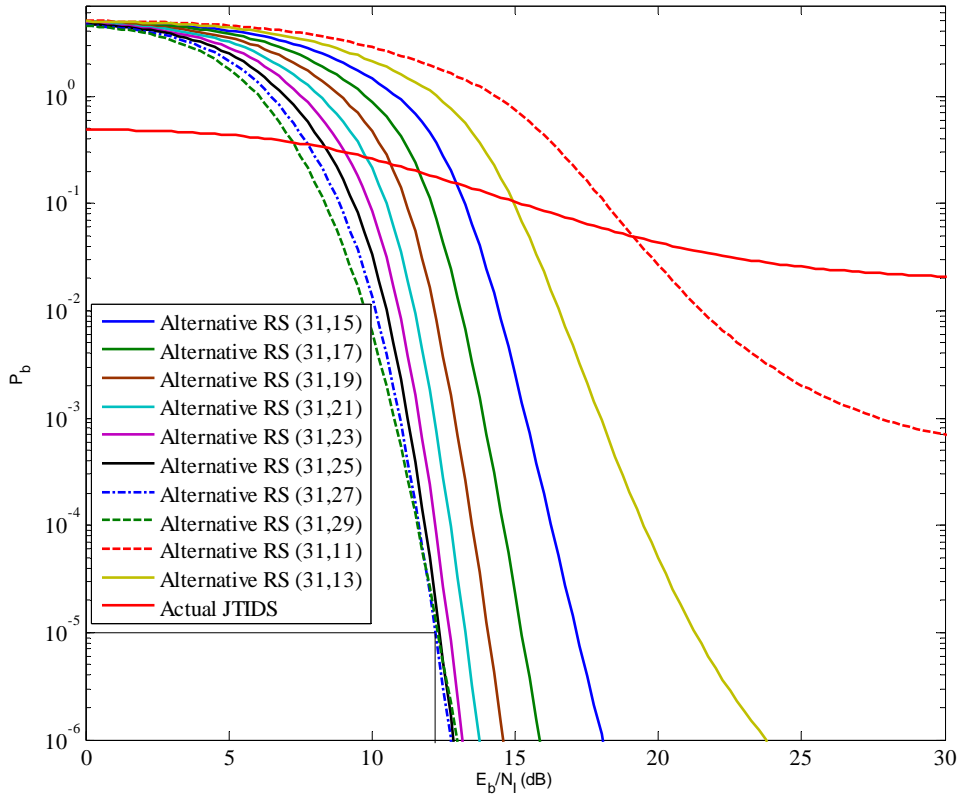
Figure 48.   Performance of 32-*ary* CCSK using concatenated coding in both AWGN and PNI for ρ=0.1, noncoherent demodulation, $E_b / N_0 = 10$ dB, diversity $L = 2$ and PSI.
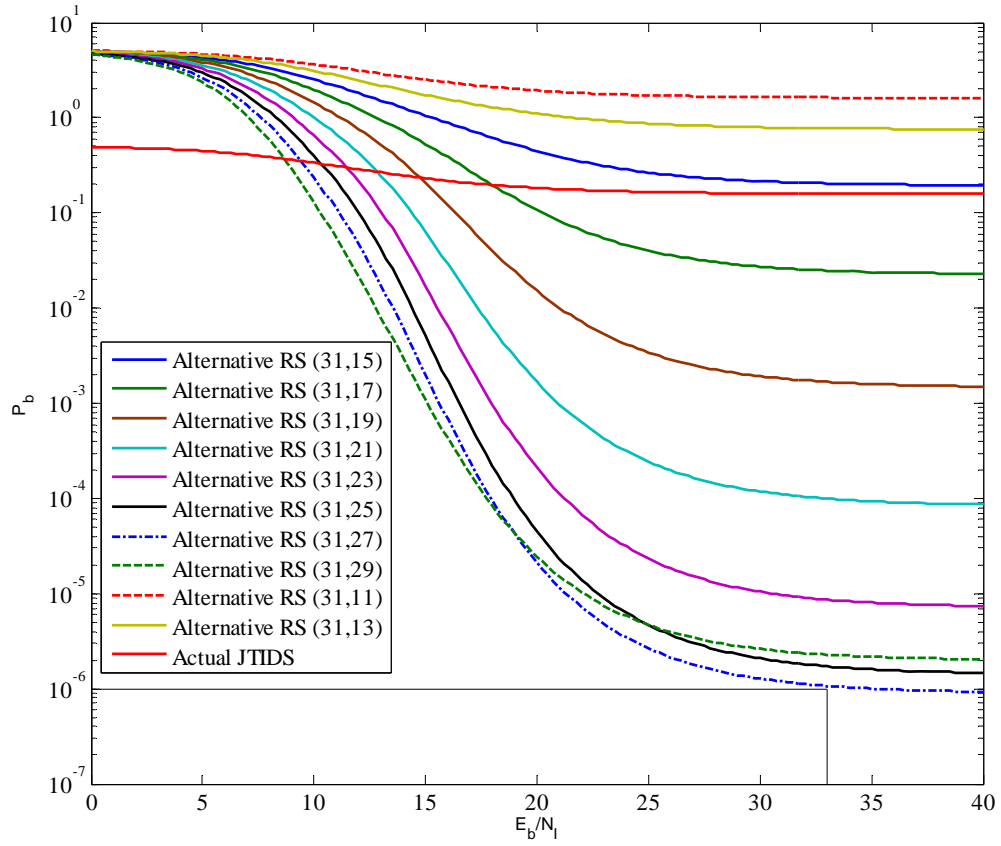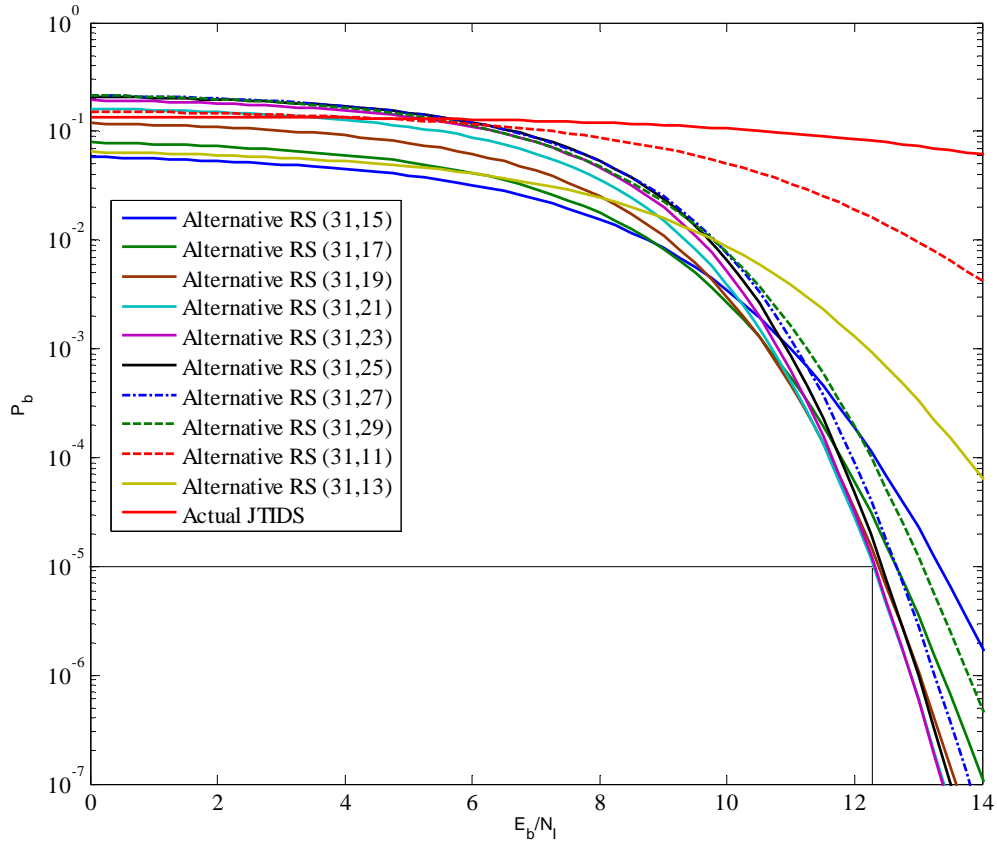
Figure 49.   Performance of 32-*ary* CCSK using concatenated coding in both AWGN and PNI for $\rho=0.1$, noncoherent demodulation, $E_b / N_0 = 8.1$ dB, diversity $L = 2$ and PSI.
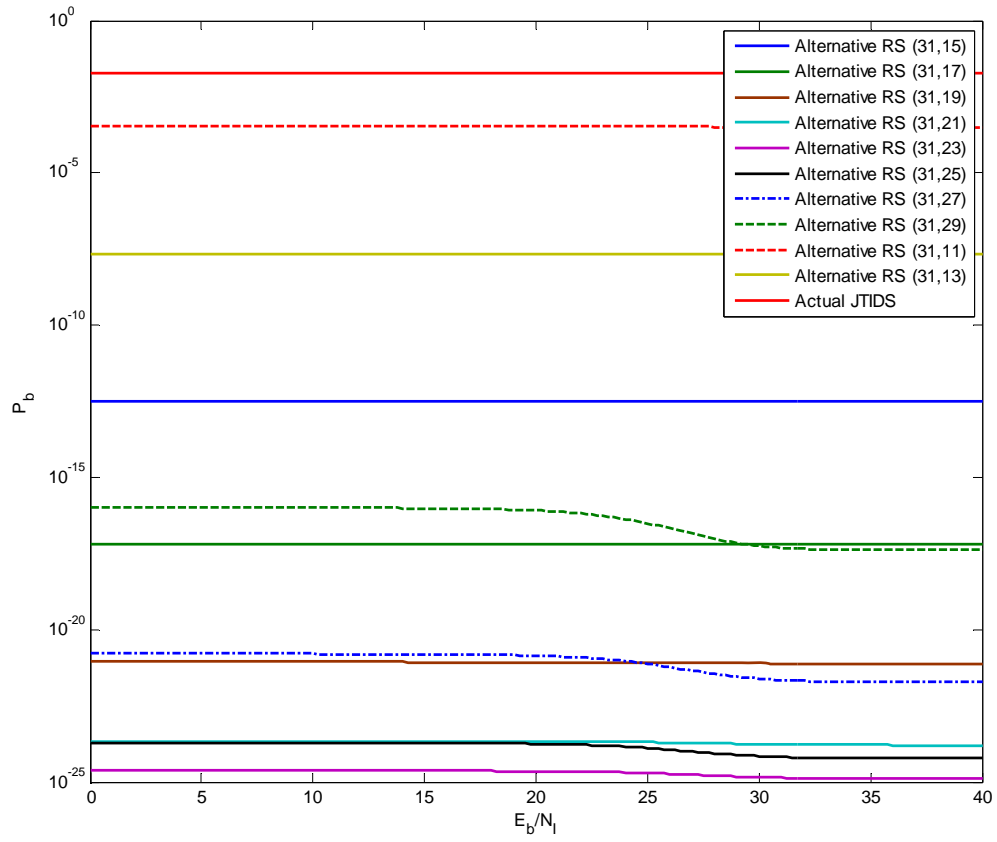
Figure 50.   Performance of 32-*ary* CCSK using concatenated coding in both AWGN and PNI for ρ=0.01, noncoherent demodulation, $E_b / N_0 = 10$ dB, diversity $L = 2$ and PSI.
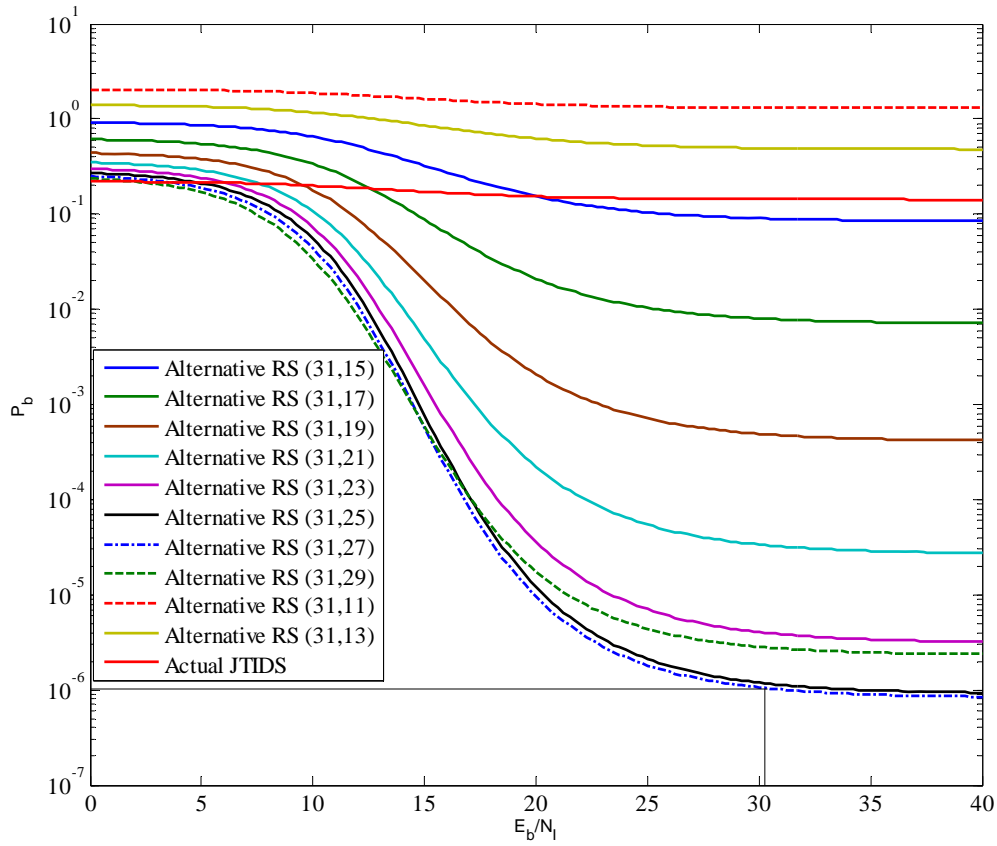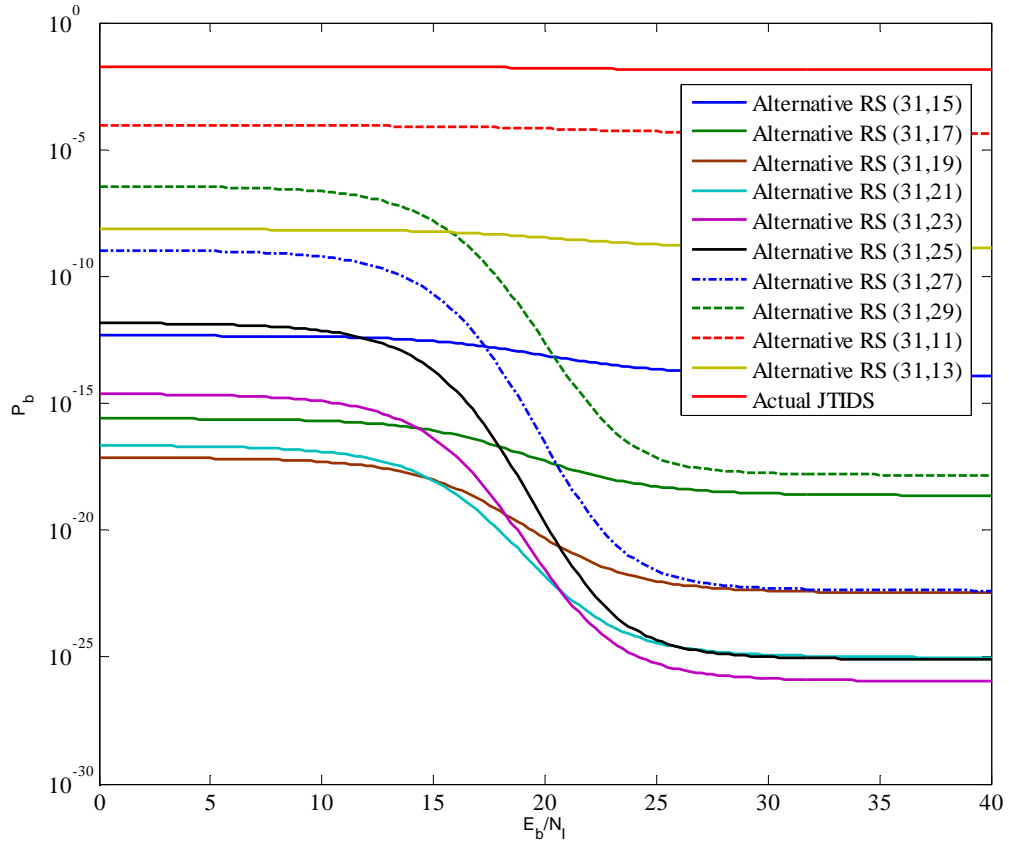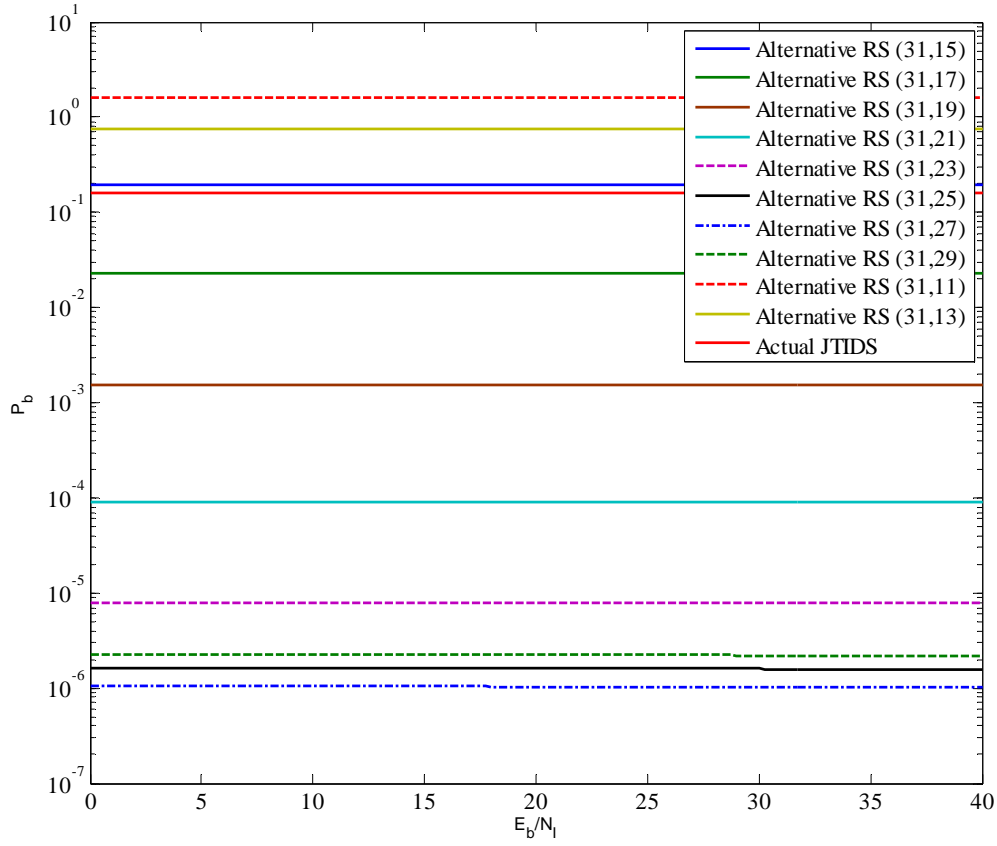
Figure 51.   Performance of 32-*ary* CCSK using concatenated coding in both AWGN and PNI for ρ=0.01, noncoherent demodulation, $E_b / N_0 = 8.1$ dB, diversity $L = 2$ and PSI.

B.   CHAPTER SUMMARY

In this chapter, the effects of AWGN and PNI on the performance of the alternative JTIDS waveform with a diversity of two for noncoherent demodulation with PSI was examined. In Chapter VII, the findings of this thesis are summarized.

THIS PAGE INTENTIONALLY LEFT BLANK

VII. CONCLUSIONS AND FUTURE WORK

A. CONCLUSIONS

This thesis presented an alternative error correction coding scheme for the physical layer waveform of the Link-16/JTIDS that is consistent with the existing JTIDS error control coding but with the potential to increase both throughput and reliability when the waveform is transmitted over a channel with PNI. The system under consideration uses a concatenated code consisting of a rate $r = 4/5$ convolutional code as the outer code and a $(31, k)$ RS code as the inner code. Both coherent and noncoherent demodulation of the proposed system were analyzed, and subsequently the performance obtained was compared with that for the existing Link-16/JTIDS waveform for AWGN as well as PNI. When only AWGN is present, the alternative waveform outperforms the Link-16/JTIDS waveform by 1.1 dB and 1.2 dB for coherent and noncoherent detection, respectively, when $P_b = 10^{-5}$. When both AWGN and PNI are present and no diversity is assumed, the improvement of the alternative waveform is at least 1.7 dB for coherent detection and at least 5.9 dB for noncoherent detection. When diversity $L = 2$ is assumed, the improvement is at least on the order of 1.8 dB. We also observed that the alternative waveform performance improvement does not come at the expense of reduced system throughput. Indeed, the throughput improvement when only AWGN is present and for coherent detection is on the order of 23%, while for noncoherent detection, throughput improvement is around 31%. Finally, when both AWGN and PNI are present the throughput improvement ranges from 17% to a maximum of 31% if the code rate is modified to require minimum signal power depending on the PNI.

When PNI is also present, we observed that, again, the alternative waveform outperforms the existing Link-16/JTIDS waveform in all the cases considered. We should mention that this improvement in required received signal power does not come at the expense of reduced throughput. Indeed, in all cases the system throughput is increased, except for the case where the double-pulse structure is coherently received in both

AWGN and PNI when $\rho \leq 0.1$ and $E_b / N_0 > 8.4$ dB. We also observed that in general the higher rate codes yield better performance for greater values of E_b / N_0, whereas lower rate codes give better performance for lower values of E_b / N_0. Additionally, we found that the double-pulse structure outperforms the single-pulse structure for $\rho \geq 0.5$, while the single-pulse structure yields better results for $\rho < 0.5$.

LIST OF REFERENCES

[1]   Dr. Carlo Kopp, "Network Centric Warfare Fundamentals-Part 3," [Online].Available at: http://www.ausairpower.net/NCW-101-3.pdf (accessed September 2009).

[2]   Dimitrios Lekkakos, "Performance Analysis of a Link-16/JTIDS Compatible Waveform Transmitted Over a Channel with Pulsed-Noise Interference," Master's thesis, Monterey, CA, September 2008.

[3]   Cheng Hoe Kee, "Performance Analysis of Alternative Link-16/JTIDS Compatible Waveforms with Complex 64-Bi-orthogonal-keyed Modulation," Master's thesis, Monterey, CA, December 2008.

[4]   Chi-Han Kao, "Performance Analysis of a JTIDS/Link-16-type Waveform Transmitted Over Slow, Flat Nakagami Fading Channels in the Presence of Narrowband Interference," Dissertation, Monterey, CA, December 2008.

[5]   P. Elias, "Coding for Noisy Channels," IRE Conv. Rec., p. 4: 37–47, 1955.

[6]   Shu Lin and Daniel J. Costello, Error Control Coding, 2nd ed., Upper Saddle River, NJ: Pearson Prentice Hall, 2004.

[7]   John G. Proakis and Masoud Salehi, Digital Communications, 4th ed., New York: McGraw-Hill, 2008.

[8]   Bernard Sklar, Digital Communications, 2nd ed., Upper Saddle River, NJ: Prentice Hall Inc., 2001.

[9]   Ralph C. Robertson, Notes for EC 4580 (Error Control Coding), Naval Postgraduate School, Monterey, CA, 2009 (unpublished).

[10]   Ralph C. Robertson, Notes for EC 4550 (Digital Communications), Naval Postgraduate School, Monterey, CA, 2009 (unpublished).

[11]   Northrop Grumman Corporation, Understanding Link-16: A Guidebook for New Users, San Diego, CA, September 2001.

[12]   Chi-Han Kao, Clark Robertson, and Kyle Lin, "Performance Analysis and Simulation of Cyclic Code-Shift Keying," Naval Postgraduate School, Monterey, CA, 2008.

[13]   Ralph C. Robertson, Notes for EC 4550 (Digital Communications-Sequential and Parallel Diversity), Naval Postgraduate School, Monterey, CA, 2009 (unpublished).

THIS PAGE INTENTIONALLY LEFT BLANK

INITIAL DISTRIBUTION LIST

1.   Defense Technical Information Center
      Ft. Belvoir, Virginia

2.   Dudley Knox Library
      Naval Postgraduate School
      Monterey, California

3.   Chairman, Code IS
      Department of Information Sciences
      Naval Postgraduate School
      Monterey, California

4.   Chairman, Code EC
      Department of Electrical and Computer Engineering
      Naval Postgraduate School
      Monterey, California

5.   Professor R. Clark Robertson, Code EC/Rc
      Department of Electrical and Computer Engineering
      Naval Postgraduate School
      Monterey, California

6.   Professor Terry Smith, Code IS/Smith
      Department of Information Sciences
      Naval Postgraduate School
      Monterey, California

7.   Embassy of Greece
      Office of Naval Attaché
      Washington, District of Columbia

8.   LTJG Koromilas Ioannis
      Hellenic Navy General Staff
      Athens, Greece